

# Endometrial aging is accompanied by H3K27ac and PGR loss

Received: 11 May 2024

Accepted: 31 March 2025

Published online: 20 May 2025

 Check for updates

Yue Wang<sup>1,2,3,4,6</sup>, Ping Zhou<sup>1,2,3,4,6</sup>, Hongying Shan<sup>1,2,3,4,6</sup>, Xiyao Liu<sup>1,2,3,4,6</sup>, Ming Cheng<sup>1,2,3,4</sup>, Zhenhong Ye<sup>1,2,3,4</sup>, Xiunan Chen<sup>1,2,3,4</sup>, Baoying Liao<sup>1,2,3,4</sup>, Tianliu Peng<sup>1,2,3,4</sup>, Chenxi Xiao<sup>1,2,3,4</sup>, Ziying Huang<sup>1,2,3,4</sup>, Yunshu Dong<sup>1,2,3,4</sup>, Yang Yu<sup>1,2,3,4,5</sup>✉, Heng Pan<sup>1,2,3,4</sup>✉ & Rong Li<sup>1,2,3,4</sup>✉

Whether and how endometrial aging affects fertility remains unclear. In our in-house clinical cohort at the Center for Reproductive Medicine of Peking University Third Hospital ( $n = 1,149$ ), we observed adverse pregnancy outcomes in the middle-aged group after excluding aneuploid embryos, implying the negative impact of endometrial aging on fertility. To understand endometrial aging, we performed comprehensive transcriptomic profiling of the mid-secretory endometrium of young (<35 years) and middle-aged ( $\geq 35$  years) patients. This analysis revealed that H3K27ac loss is linked to impaired endometrial receptivity in the middle-aged group. We eliminated H3K27ac in young human endometrial stromal cells and observed reduced progesterone receptor (PGR), a critical regulator of endometrial receptivity. Lastly, we validated the association between H3K27ac/PGR loss and uterine aging in a mouse model. Our findings establish H3K27ac as a critical regulator of PGR and demonstrate that endometrial H3K27ac loss is associated with aging-related fertility decline. This work provides valuable insights into enhancing the safety and efficacy of assisted reproductive technologies in future clinical practices.

Due to the social advancement and lifestyle changes, there has been a rise in the number of persons conceiving in their late 30s, leading to frequent concerns about the impact of advanced maternal age (AMA) on pregnancies<sup>1–4</sup>. Aging is associated with adverse pregnancy outcomes, including fertility decline, miscarriage, fetal growth restriction, stillbirth and preeclampsia<sup>5–8</sup>. Although the aging-related decline in the quality of oocytes and embryos is a major causal factor of infertility<sup>9,10</sup>, the effect of the aging endometrium remains controversial<sup>10–13</sup>. Understanding the underlying mechanisms of endometrial aging and its impact on fertility is crucial for the effective treatment of aging-related female-factor infertility.

Embryo implantation is the most critical step of the reproductive process in many species<sup>14</sup>, requiring the sophisticated cross-talk between the implantation-competent blastocyst and receptive endometrium<sup>15,16</sup>. Endometrial receptivity is a complex process that allows the embryo to attach, invade and develop in a specific period known as the window of implantation (WOI) or mid-secretory phase<sup>17–19</sup>. The endometrium undergoes considerable structural and functional changes during the WOI<sup>20</sup>. Growth factors, hormones, prostaglandins, adhesion molecules, nuclear receptors and epigenetic modifications tightly regulate endometrial receptivity<sup>21–24</sup>. In addition to classical nuclear receptors, such as progesterone receptor (PGR) and estrogen

<sup>1</sup>State Key Laboratory of Female Fertility Promotion, Center for Reproductive Medicine, Department of Obstetrics and Gynecology, Peking University Third Hospital, Beijing, China. <sup>2</sup>National Clinical Research Center for Obstetrics and Gynecology, Peking University Third Hospital, Beijing, China. <sup>3</sup>Key Laboratory of Assisted Reproduction, Peking University, Ministry of Education, Beijing, China. <sup>4</sup>Beijing Key Laboratory of Reproductive Endocrinology and Assisted Reproductive Technology, Beijing, China. <sup>5</sup>Beijing Advanced Center of Cellular Homeostasis and Aging-Related Diseases, Institute of Advanced Clinical Medicine, Peking University, Beijing, China. <sup>6</sup>These authors contributed equally: Yue Wang, Ping Zhou, Hongying Shan, Xiyao Liu. ✉e-mail: [yuyang5012@hotmail.com](mailto:yuyang5012@hotmail.com); [hep2007@bjmu.edu.cn](mailto:hep2007@bjmu.edu.cn); [roseli001@sina.com](mailto:roseli001@sina.com)

receptor (ER $\alpha$ )<sup>25</sup>, accurate histone modifications are also necessary for embryo implantation, enabling essential gene expression for decidualization, such as *WNT4*, *ZBTB16*, *PROK1* and *GREB1* (refs. 24,26). As a histone modification linked to transcriptional activation, H3K27ac increases in human endometrial stromal cells during decidualization with the accumulation in the distal upstream region of *IGFBP1*, activating its expression<sup>27,28</sup>. Nevertheless, the impact of H3K27ac on endometrial receptivity and its relevance to endometrial aging remain elusive.

In this study, we first confirmed the aging-related adverse impact of the endometrium on fertility based on pregnancy outcomes of a clinical cohort at the Center for Reproductive Medicine of Peking University Third Hospital ( $n = 1,149$ ). Next, we characterized H3K27ac patterns in the mid-secretory endometrium of middle-aged patients, illustrating that H3K27ac loss is closely associated with PGR depletion and impaired endometrial receptivity, which was validated in a mouse model. Eliminating H3K27ac in young human endometrial stromal cells and young murine uteri reduced PGR expression. However, PGR inhibition did not affect H3K27ac in the mouse, indicating that H3K27ac is the upstream regulator of PGR. In summary, we identify H3K27ac loss as one of the hallmarks of endometrial aging, confirm the cooperatively regulatory roles of H3K27ac and PGR on genes and pathways relevant to endometrial receptivity and provide potential treatment strategies to improve reproductive outcomes in AMA pregnancies.

## Results

### Aging endometrium exhibits impaired endometrial receptivity

To investigate the impact of endometrial aging on pregnancy outcomes, we collected the clinical information of 1,149 patients who had undergone pre-implantation genetic testing for aneuploidy (PGT-A) screening at the Center for Reproductive Medicine of Peking University Third Hospital (Fig. 1a and Supplementary Table 1). After excluding embryonic aneuploidy, the rates of biochemical pregnancy, clinical pregnancy and live birth were significantly lower in the middle-aged group (Fig. 1b), implying the adverse impact of endometrial aging on fertility.

Impaired endometrial receptivity is one of the hallmarks of endometrial disorder, featuring extensive morphological and molecular changes<sup>13</sup>. Changes in epithelial and stromal cells are necessary to establish endometrial receptivity and synchronize the endometrium with embryo implantation<sup>29</sup>. We observed the abnormal proliferation of epithelial cells and dysregulated decidual function of stromal cells in middle-aged patients (Fig. 1c–f, Extended Data Fig. 1a,b and Supplementary Tables 2 and 3). Aging stromal cells failed to develop the typical morphology of decidual cells upon cyclic adenosine monophosphate (cAMP) and medroxyprogesterone acetate (MPA) treatment (Fig. 1d). Decidual markers, including PRL and *IGFBP1*, were significantly decreased in the middle-aged group during decidualization (Fig. 1e,f and Extended Data Fig. 1b).

We next focused on classic steroid hormone receptors PGR and ER $\alpha$ , which are central regulators of endometrial receptivity. PGR and

ER $\alpha$  were significantly reduced in the mid-secretory endometrium of middle-aged patients (Fig. 1g–j and Extended Data Fig. 1c–e). Their reductions in the middle-aged group were also confirmed in isolated endometrial epithelial and stromal cells (Extended Data Fig. 1f–k). To determine the transcriptional signature of endometrial aging, we applied RNA sequencing (RNA-seq) to the mid-secretory endometrium of young ( $n = 10$ ) and middle-aged ( $n = 8$ ) patients (Supplementary Table 2). The endometrium of the middle-aged group showed a distinct gene expression profile compared to young participants, with a substantial downregulation of *PGR* and other positive regulators of endometrial receptivity (Fig. 1k,l and Extended Data Fig. 1l–p). Downregulated differentially expressed genes (DEGs) in the endometrium of middle-aged patients were enriched in the pathways of the mitotic cell cycle, cell cycle and G1/S transition (Fig. 1l). We also applied RNA-seq to isolated epithelial and stromal cells of the mid-secretory endometrium ( $n = 4$  for each group) to characterize transcriptomic changes along with aging in the cell-type-specific manner (Supplementary Table 4). Gene expression profiles differed between the young and middle-aged groups in both epithelial and stromal cells (Extended Data Fig. 2). However, aging-related transcriptional changes varied between epithelial and stromal cells. Changes in stromal cells were more similar to the endometrium, including the downregulation of genes in the pathways of the mitotic cell cycle and cell cycle in the middle-aged group (Extended Data Fig. 2d), considering that most endometrial cells were stromal cells (>60%, estimated by CIBERSORTx)<sup>30</sup>. Genes related to cell proliferation were upregulated in endometrial epithelial cells of the middle-aged group (Extended Data Fig. 2j), consistent with excessive epithelial proliferation.

Our observations revealed abnormal cell morphologies, hormonal responses and cell proliferation in the endometrium of middle-aged patients, which are associated with impaired endometrial receptivity.

### Aging-related H3K27ac loss is associated with PGR reduction

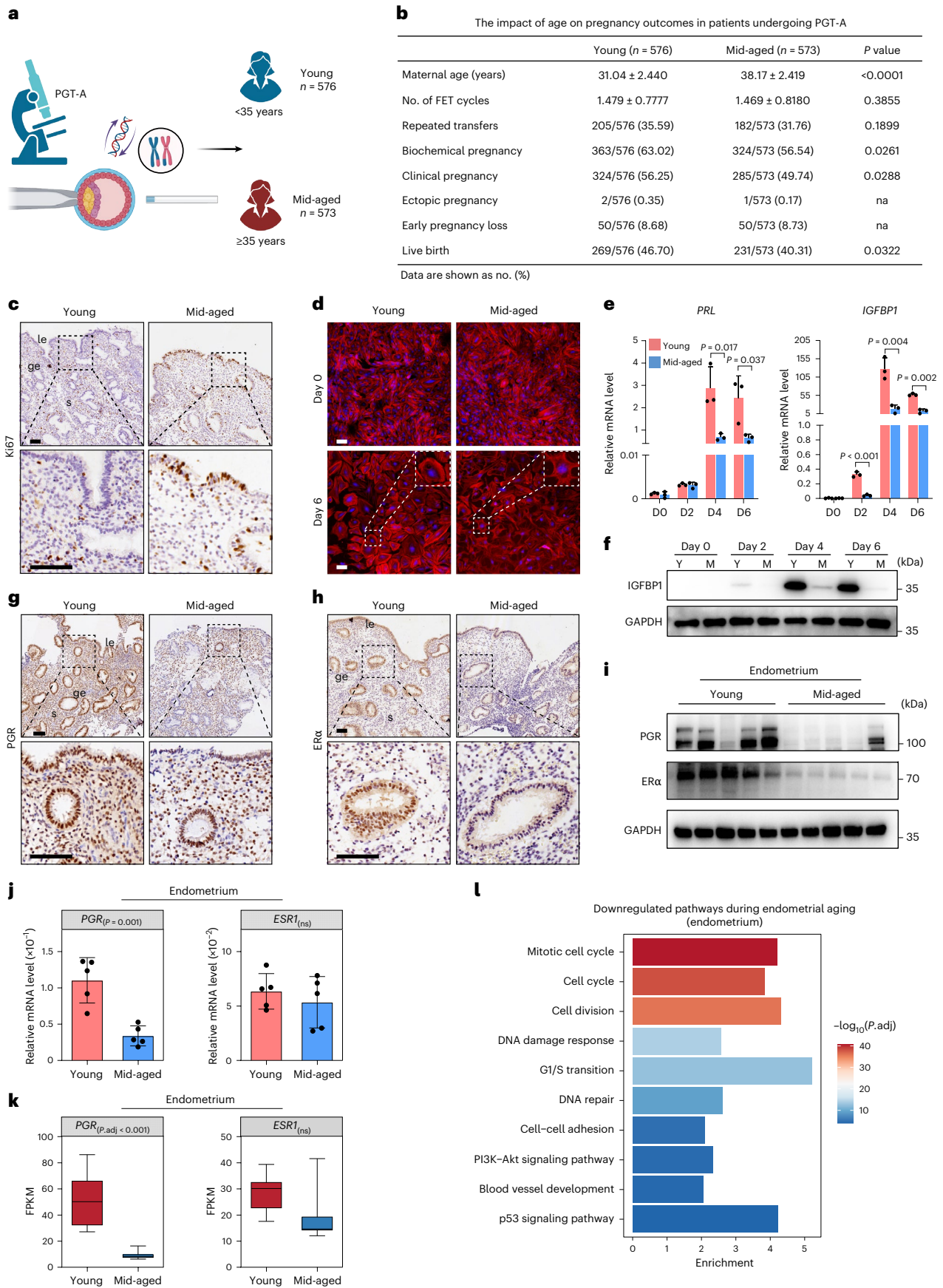
We evaluated the overlap between aging-related DEGs and genes marked by different histone modifications to identify upstream regulators. Endometrial DEGs were significantly enriched in genes marked by H3K27ac or H3K27me3 (Fig. 2a). Unlike H3K27me3, the impact of H3K27ac on endometrial receptivity remains unclear<sup>31</sup>. Of note, genes encoding H3K27ac writers and readers were downregulated in the mid-secretory endometrium of middle-aged patients, whereas genes encoding erasers were upregulated (Fig. 2b), consistent with the reduced H3K27ac level in both aging epithelial and stromal cells (Fig. 2c–e). A significantly lower level of H3K27ac in the proliferative phase reassured that H3K27ac may primarily exert its function in the mid-secretory phase (Extended Data Fig. 3a–c). We, thus, speculate that H3K27ac loss is relevant to impaired endometrial receptivity in middle-aged patients.

We next conducted CUT&Tag to explore the genomic distribution of H3K27ac in endometrial epithelial and stromal cells of young and

### Fig. 1 | Aging endometrium exhibits impaired endometrial receptivity.

**a**, Schematic design to assess pregnancy outcomes of young and middle-aged patients undergoing PGT-A. **b**, The impact of age on pregnancy outcomes in patients undergoing PGT-A. **c**, Representative images showing Ki67 immunohistochemistry (IHC) staining in the human mid-secretory endometrium ( $n = 3$ ). **d**, Immunofluorescence (IF) staining of cell morphologies in human endometrial stromal cells during induced decidualization. Decidualization was induced by the treatment of 0.5  $\mu$ M cAMP and 1  $\mu$ M MPA. The F-actin cytoskeleton was visualized by rhodamine phalloidin staining. **e**, Relative mRNA levels of *IGFBP1* and *PRL* in human endometrial stromal cells during induced decidualization ( $n = 3$ ). **f**, Representative images illustrating protein levels of *IGFBP1* in human endometrial stromal cells during induced decidualization ( $n = 3$ ). **g**, Representative images showing PGR IHC staining in the human mid-secretory endometrium ( $n = 3$ ). **h**, Representative images showing ER $\alpha$  IHC staining in the human mid-secretory endometrium ( $n = 3$ ). **i**, Protein levels

of PGR and ER $\alpha$  in the human mid-secretory endometrium ( $n = 5$ ). **j**, Relative mRNA levels of *PGR* and *ESR1* in the human mid-secretory endometrium ( $n = 5$ ). **k**, FPKM of *PGR* and *ESR1* in the human mid-secretory endometrium ( $n = 10$  and  $n = 8$  for the young and middle-aged groups, respectively). The adjusted  $P$  value was determined by DESeq2 (ref. 79). The median, upper and lower quartiles are shown. Whiskers represent upper quartile + 1.5 interquartile range (IQR) and lower quartile – 1.5 IQR. **l**, Pathway enrichment analysis of downregulated DEGs in the aging mid-secretory endometrium. The adjusted  $P$  value was determined by Metascape<sup>80</sup>. In **c**, **d**, **g** and **h**, scale bar, 50  $\mu$ m. The nuclei were stained with hematoxylin in the IHC staining and with DAPI in the IF staining. In **e** and **j**, statistical analysis was performed by two-sided unpaired Student's  $t$ -test. Data are presented as mean  $\pm$  s.d. All replicates were biological replicates. D, day; FPKM, fragments per kilobase of transcript per million mapped reads; ge, glandular epithelium; le, luminal epithelium; M or mid-aged, middle-aged; na, not applicable; ns, not significant;  $P$ .adj, adjusted  $P$  value; s, stroma; Y, young.



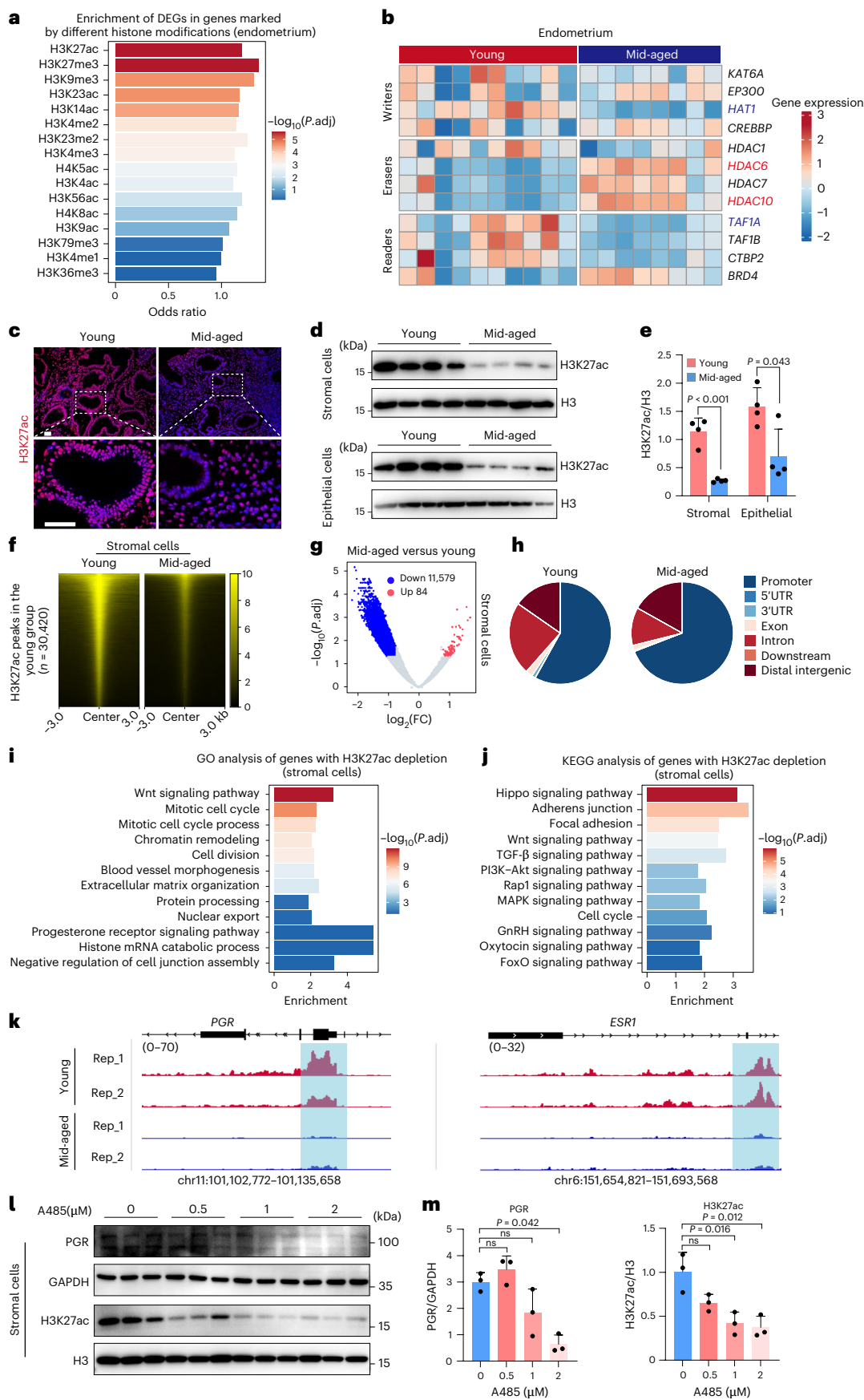


**Fig. 2 | Aging-related H3K27ac loss is associated with PGR reduction.**

**a**, Enrichment of aging-related endometrial DEGs in genes marked by different histone modifications. **b**, Heatmaps showing endometrial gene expression of H3K27ac writers, erasers and readers. Red and blue gene symbols represent aging-related upregulated and downregulated DEGs separately. **c**, H3K27ac immunofluorescence (IF) staining in the human mid-secretory endometrium. Scale bar, 50  $\mu\text{m}$ . The nuclei were stained with DAPI. **d**, The H3K27ac level in human mid-secretory endometrial stromal and epithelial cells ( $n = 4$ ). **e**, The relative H3K27ac level in human mid-secretory endometrial stromal and epithelial cells ( $n = 4$ ). **f**, Heatmaps of the H3K27ac signal in human mid-secretory endometrial stromal cells at H3K27ac peaks in the young group. **g**, Volcano plot illustrating H3K27ac differences between young and aging mid-secretory endometrial stromal cells. Red and blue points represent peaks that gain and lose H3K27ac in aging stromal cells. **h**, The genomic distribution of H3K27ac peaks

in human mid-secretory endometrial stromal cells. **i**, GO enrichment analysis of genes with H3K27ac loss in aging mid-secretory endometrial stromal cells. **j**, KEGG enrichment analysis of genes with H3K27ac loss in aging mid-secretory endometrial stromal cells. **k**, The H3K27ac signal in mid-secretory endometrial stromal cells at selected genes. hg38 coordinates are shown. The blue shading indicates the specific region with H3K27ac loss in the middle-aged group. **l**, H3K27ac and PGR levels in mid-secretory endometrial stromal cells after treatment with A485 ( $n = 3$ ). **m**, Relative H3K27ac and PGR levels in mid-secretory endometrial stromal cells after treatment with A485 ( $n = 3$ ). In **e** and **m**, statistical analysis was performed by two-sided unpaired Student's *t*-test or Mann–Whitney *U*-rank-sum test (when data did not follow a normal distribution). Data are presented as mean  $\pm$  s.d. All replicates were biological replicates. FC, fold change; GO, Gene Ontology; KEGG, Kyoto Encyclopedia of Genes and Genomes; mid-aged, middle-aged; ns, not significant; *P*.adj, adjusted *P* value; UTR, untranslated region.

middle-aged patients ( $n = 3$  for each group) and to understand the association between H3K27ac loss and impaired endometrial receptivity (Extended Data Fig. 3d and Supplementary Table 4). H3K27ac peaks of biological replicates were merged, considering their consistency with each other (Extended Data Fig. 3e,f). In stromal cells, we observed thousands of differentially binding peaks, with H3K27ac loss in most peaks and genes in the middle-aged group (Fig. 2f,g and Extended Data Fig. 3g). As an important transcriptional activator<sup>32,33</sup>, H3K27ac was prevalent at the transcription start site (TSS) compared to other genomic regions (Fig. 2h and Extended Data Fig. 3g). We observed fewer H3K27ac peaks in epithelial cells, and there were almost no differentially binding peaks between the two groups (Extended Data Fig. 3h–j). Therefore, we only focused on stromal cells for downstream analysis. In stromal cells, genes marked by H3K27ac exhibited enrichment in the Wnt and BMP signaling pathways (Extended Data Fig. 3k), which are crucial for stromal cell proliferation and differentiation during implantation<sup>34–37</sup>. Aging-related H3K27ac loss happened around genes involved in signaling pathways relevant to endometrial receptivity (Fig. 2i,j). For instance, we observed eliminated H3K27ac in the promoter region of *PGR* and *ESRI* (not the representative transcript of *ESRI*) in the middle-aged group (Fig. 2k). Compared to ER $\alpha$ , aging-related expression changes in PGR in endometrial stromal cells showed a greater magnitude (log<sub>2</sub> fold change, PGR versus ER $\alpha$ : qRT-PCR,  $-1.00$  versus  $-0.70$ ; RNA-seq,  $-1.99$  versus  $-0.42$ ; western blot,  $-0.48$  versus  $-0.29$ ). Thus, PGR was selected as the downstream target of H3K27ac for further exploration. To validate the causal relationship between H3K27ac and PGR, we applied different concentrations of A485 (an inhibitor of p300, a writer of H3K27ac) after 24 h of culture to eliminate H3K27ac in young endometrial stromal cells ( $n = 3$  for each group). When treated with 2  $\mu\text{M}$  A485, PGR was significantly downregulated upon H3K27ac reduction (Fig. 2l,m), confirming that eliminating H3K27ac in young endometrial stromal cells reduces PGR.

**H3K27ac and PGR regulate endometrial receptivity together**

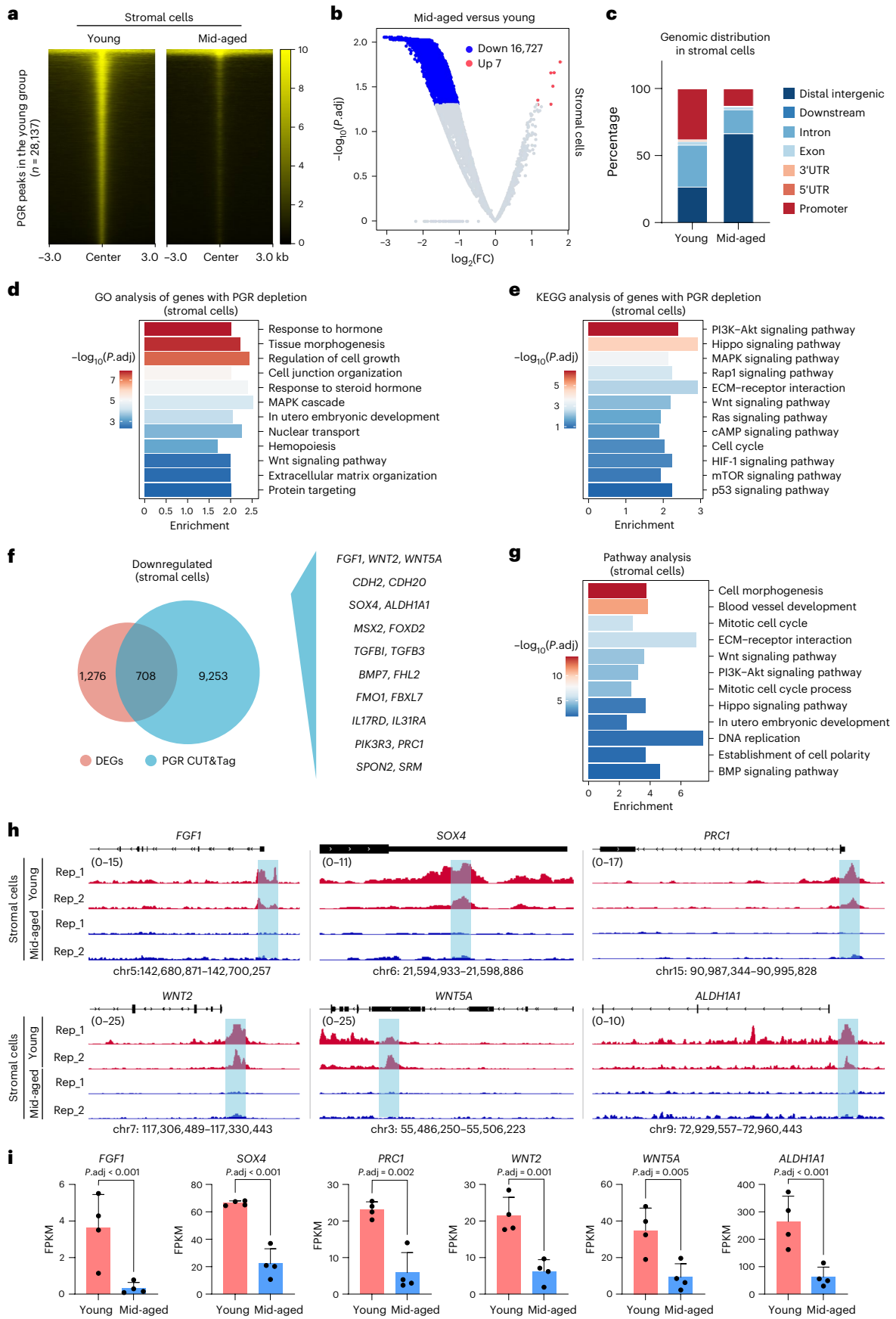
We further explored the genomic distribution of PGR in human endometrial stromal cells. PGR CUT&Tag was applied to endometrial stromal cells of young and middle-aged patients ( $n = 3$  for each group; Supplementary Table 4). PGR binding peaks of biological replicates

were merged, considering their consistency with each other (Extended Data Fig. 4a). Consistent with lower PGR expression in aging endometrial stromal cells, we observed genome-wide depletion of PGR binding (Fig. 3a,b and Extended Data Fig. 4b). As an important transcription factor, PGR binding in the young group and PGR depletion in the middle-aged group were both prevalent around promoters (Fig. 3c and Extended Data Fig. 4b). Genes with PGR depletion in aging stromal cells were primarily enriched in pathways associated with endometrial receptivity, such as the Wnt signaling pathway<sup>34,35</sup> (Fig. 3d,e and Extended Data Fig. 4c,d). These observations revealed that aging-related abnormal PGR recruitment was relevant to impaired endometrial receptivity. To further investigate associations among PGR depletion, gene repression and impaired endometrial receptivity, we selected downregulated genes with simultaneous PGR depletion in aging stromal cells and performed pathway enrichment analysis (Fig. 3f,g). These genes were prevalent in pathways relevant to cell proliferation, differentiation and endometrial receptivity, such as the ECM–receptor interaction, and the Wnt, BMP and Hippo signaling pathways<sup>34,38,39</sup> (Fig. 3g). Dysregulated Wnt and ECM signaling pathways were reported to lead to abnormal proliferation and differentiation of endometrial cells<sup>40–42</sup>. Representative genes of these pathways, such as *FGF1*, *SOX4*, *PRC1*, *WNT2*, *WNT5A* and *ALDH1A1*, showed gene repression and PGR depletion at the same time (Fig. 3h,i).

Given that H3K27ac loss was associated with PGR depletion and abnormal endometrial receptivity, a new question is whether H3K27ac and PGR cooperatively regulate genes relevant to endometrial receptivity. We observed correlative genomic occupancies between PGR and H3K27ac (Fig. 4a–d). This co-localization was consistent along gene bodies and the entire genome (Fig. 4c,d), which was further confirmed by motif analysis and the co-immunoprecipitation (co-IP) experiment between PGR and p300 (Fig. 4e,f). Aging-related H3K27ac loss and PGR depletion also occurred at similar genomic regions (Fig. 4g), affecting key regulators of endometrial receptivity together, such as *FOXO1*, *HOXA10* and *HAND2* (Fig. 4h,i). These genes were significantly downregulated in the middle-aged group, along with H3K27ac and PGR loss (Fig. 4j,k and Extended Data Fig. 4e). Genes that exhibited simultaneous depletion of both PGR and H3K27ac in the middle-aged group were enriched in the Wnt and MAPK signaling pathways, revealing abnormal

**Fig. 3 | Aging endometrium shows genome-wide PGR depletion.** **a**, Heatmaps of the PGR signal in human mid-secretory endometrial stromal cells at PGR peaks in the young group. **b**, Volcano plot illustrating PGR differences between young and aging mid-secretory endometrial stromal cells. Red and blue points represent peaks that gain and lose the PGR signal in aging stromal cells. **c**, The genomic distribution of PGR peaks in human mid-secretory endometrial stromal cells. **d**, GO enrichment analysis of genes with PGR depletion in aging mid-secretory endometrial stromal cells. **e**, KEGG enrichment analysis of genes with PGR depletion in aging mid-secretory endometrial stromal cells. **f**, Venn diagram illustrating the overlap between downregulated DEGs and genes with

PGR depletion in aging mid-secretory endometrial stromal cells. **g**, Pathway enrichment analysis of 708 common genes indicated in **f**. **h**, The PGR signal in mid-secretory endometrial stromal cells at selected genes. hg38 coordinates are shown. The blue shading indicates the specific region with PGR depletion in the middle-aged group. **i**, FPKM of selected genes in human mid-secretory endometrial stromal cells ( $n = 4$ ). The adjusted *P* value was determined by DESeq2 (ref. 79). Data are presented as mean  $\pm$  s.d. All replicates were biological replicates. FC, fold change; FPKM, fragments per kilobase of transcript per million mapped reads; GO, Gene Ontology; KEGG, Kyoto Encyclopedia of Genes and Genomes; mid-aged, middle-aged; *P*.adj, adjusted *P* value; UTR, untranslated region.



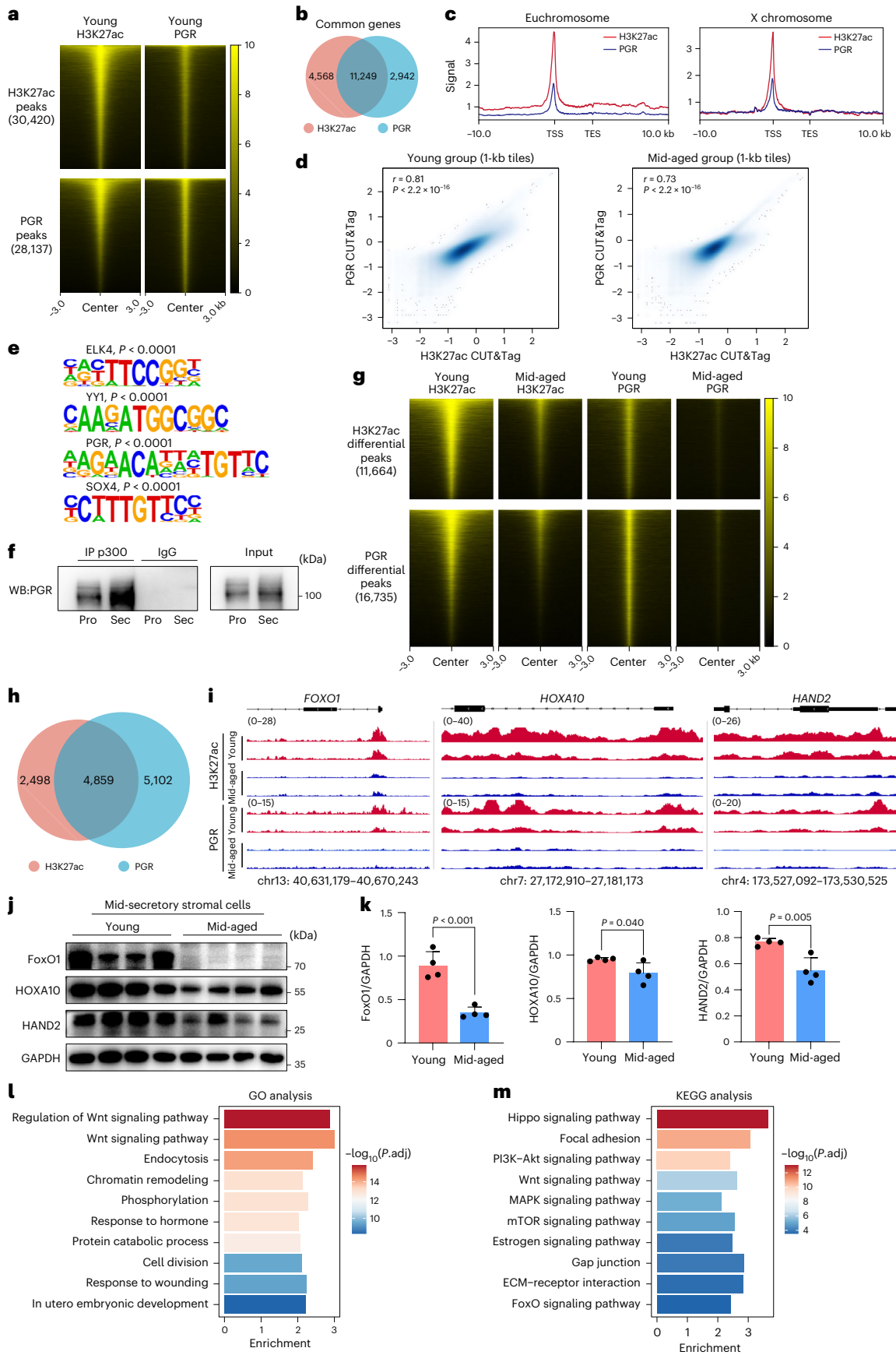


**Fig. 4 | H3K27ac and PGR exhibit correlated genomic occupancies and coordinated aging-related depletion.** **a**, Heatmaps of H3K27ac and PGR signals in young mid-secretory endometrial stromal cells at H3K27ac and PGR peaks in the young group. **b**, Venn diagram illustrating the overlap between genes marked by H3K27ac and PGR. **c**, The H3K27ac and PGR signals in young mid-secretory endometrial stromal cells at the euchromosome and X chromosome. **d**, One-kilobase plots showing the correlation between H3K27ac and PGR signals in human mid-secretory endometrial stromal cells. **e**, Motif analysis of H3K27ac peaks in young mid-secretory endometrial stromal cells. **f**, Co-IP assays showing the interaction between p300 and PGR in the human endometrium. **g**, Heatmaps of H3K27ac and PGR signals in human mid-secretory endometrial stromal cells at differentially binding peaks of H3K27ac and PGR between the two groups.

**h**, Venn diagram illustrating the overlap between genes with H3K27ac and PGR loss. **i**, H3K27ac and PGR signals in mid-secretory endometrial stromal cells at selected genes. hg38 coordinates are shown. **j**, Protein levels of FoxO1, HOXA10 and HAND2 in mid-secretory endometrial stromal cells ( $n = 4$ ). **k**, Relative protein levels of FoxO1, HOXA10 and HAND2 in mid-secretory endometrial stromal cells ( $n = 4$ ). Statistical analysis was performed by two-sided unpaired Student's  $t$ -test. Data are presented as mean  $\pm$  s.d. **l**, GO enrichment analysis of genes with H3K27ac and PGR loss. **m**, KEGG enrichment analysis of genes with H3K27ac and PGR loss. All replicates were biological replicates. GO, Gene Ontology; KEGG, Kyoto Encyclopedia of Genes and Genomes; mid-aged, middle-aged;  $P$ .adj, adjusted  $P$  value; Pro, proliferative phase; Sec, secretory phase; TES, transcription end site; WB, western blot.

endometrial receptivity<sup>35,43</sup> (Fig. 4l,m). Our results indicated a collaborative relationship between H3K27ac and PGR, regulating genes related to endometrial receptivity cooperatively. This finding is unlikely due to technical artifacts because we also identified genomic regions that gain H3K27ac but lose PGR (Extended Data Fig. 4f).

### Eliminating H3K27ac impairs murine uterine receptivity

To functionally validate that aging-related endometrial H3K27ac loss impairs fertility by reducing PGR, we used an aging mouse model (10-month-old C57BL/6J mice). It was reported that the total number of pups and the average number of pups per litter in aging mice were significantly lower than in young mice<sup>44–46</sup>, indicating impaired uterine receptivity. Consistently, our aging mice exhibited abnormal uterine receptivity with excessive proliferation of uterine luminal epithelial cells and decreased uterine H3K27ac on day 4 (Fig. 5a–c and Extended Data Fig. 5a,b). Aging murine uteri also showed distinct gene expression patterns compared to the young group (Fig. 5d and Extended Data Fig. 5c–f). Aging-related transcriptional changes were consistent between the human endometrium and the murine uterus (Fig. 5d–f). For instance, several pathways, including the cell cycle, G1/S transition and mitotic cell cycle, were enriched with aging-related downregulated genes in both humans and mice (Figs. 1l and 5d,e). Genes downregulated in the endometrium of middle-aged patients tended to be also downregulated in the aging murine uterus (Fig. 5f). These observations confirmed the reliability of using mice as the validation model.

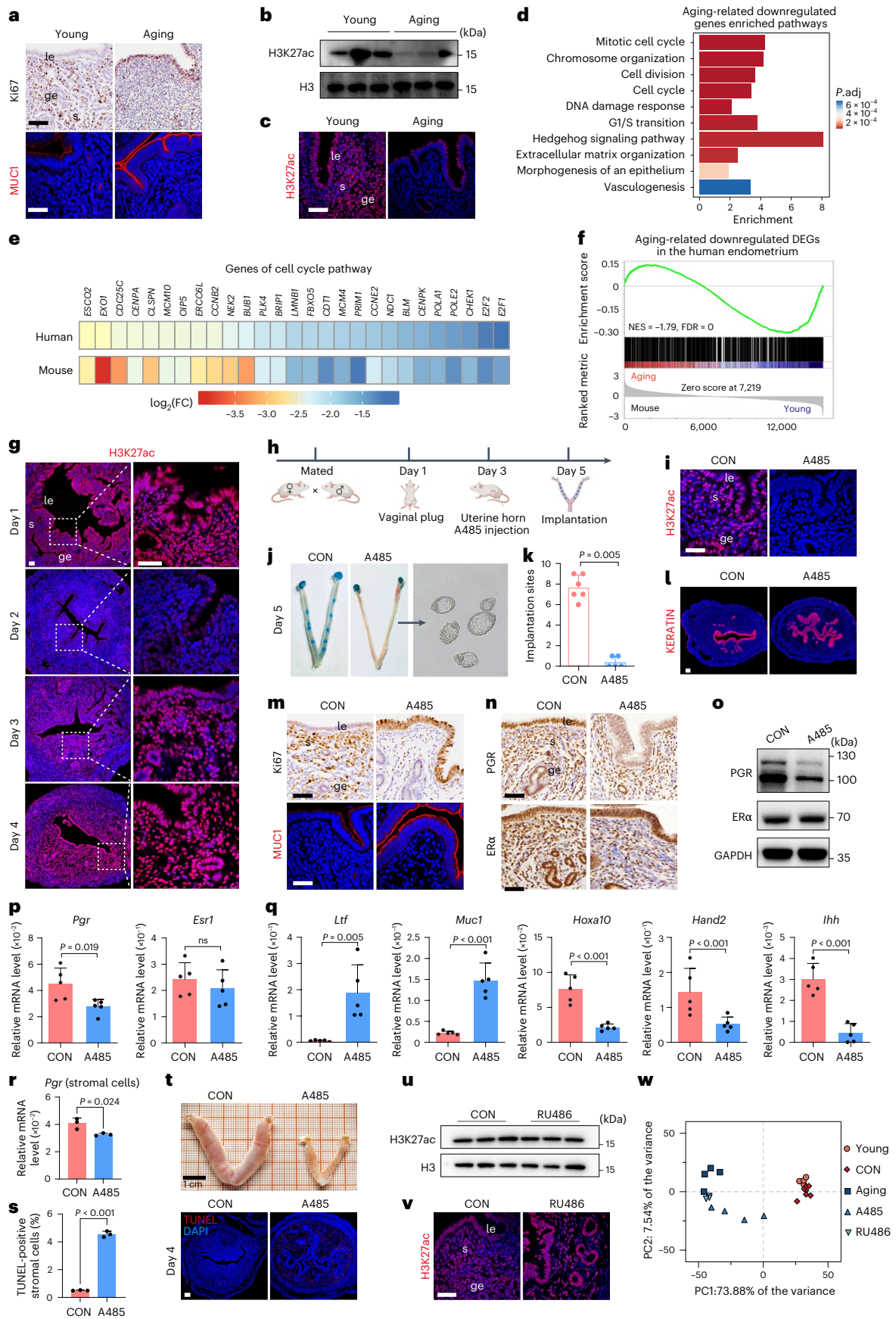
We observed high H3K27ac in both uterine epithelial and stromal cells during the peri-implantation stage (day 4), when the uterus is in the receptive state, suggesting that H3K27ac is closely associated with endometrial receptivity and embryo implantation (Fig. 5g). To investigate whether H3K27ac loss impairs uterine receptivity, we injected 5  $\mu$ l of 100  $\mu$ M A485 into the uterine horn on day 3 of the pregnancy, and H3K27ac was effectively eliminated on day 4 (Fig. 5h,i). A485 mice exhibited implantation failure on day 5, along with abnormal proliferation of epithelial cells and uterine dysfunction (a defective luminal closure characterized by increased luminal epithelial branches), but without observed blastocyst alterations (Fig. 5j–m and Extended Data

Fig. 6a–e). Blastocysts that failed to implant were observed in the uterine lumen in the A485 group (Fig. 5j). PGR expression was decreased in the A485 group, whereas ER $\alpha$  remained unaffected (Fig. 5n–p and Extended Data Fig. 6f,g). Next, RNA-seq was performed on the control and A485 uterine samples on day 4. We observed distinct transcriptional profiles between the control and A485 groups, resembling the aging process (Extended Data Fig. 6h–l). Progesterone-responsive genes, such as *Hoxa10*, *Hand2* and *Ihh*, were downregulated in the A485 group along with PGR depletion (Fig. 5p,q). Estrogen-responsive genes *Ltf* and *Muc1* were upregulated even though ER $\alpha$  was unaffected (Fig. 5p,q), which might be due to the imbalance between progesterone and estrogen caused by PGR depletion. The impact of H3K27ac loss on PGR was further evaluated in uterine stromal cells specifically. Upon A485 treatment, murine uterine stromal cells showed decreased *Pgr* expression, increased apoptosis rate and defective decidualization (Fig. 5r–t). It was reported that abnormal stromal cell proliferation and apoptosis impair endometrial receptivity<sup>47–49</sup>. Of note, decidualization is different between humans and mice. The human decidua is formed routinely and is shed off in the absence of an embryo<sup>50</sup>. However, in mice, decidualization of stromal cells occurs after successful embryo implantation<sup>50,51</sup>. Nonetheless, we still identified a conserved mechanism between humans and mice: H3K27ac regulates PGR expression in stromal cells and, thus, affects endometrial/uterine receptivity.

To further characterize the relationship between PGR and H3K27ac, antiprogestosterone RU486 was injected into the uterine horn on day 3, whereas the control group was administered with DPBS. Progesterone-responsive genes, such as *Hand2*, *Hoxa10* and *Ihh*, were significantly decreased in the RU486 group, confirming the effective interference of PGR (Extended Data Fig. 7a). PGR disruption also resulted in dramatic transcriptional changes (Extended Data Fig. 7b–f), similar to the aging process. However, those aging-like changes were not accompanied by H3K27ac loss or significant expression changes of H3K27ac writers and erasers (Fig. 5u,v and Extended Data Fig. 7g,h). Thus, we conclude that H3K27ac is an upstream factor regulating PGR in the receptive murine uterus, whereas PGR cannot affect H3K27ac reversely.

**Fig. 5 | Eliminating H3K27ac impairs murine uterine receptivity.** **a**, Ki67 immunohistochemistry (IHC) and MUC1 immunofluorescence (IF) staining in the murine uterus on day 4. **b**, H3K27ac in the murine uterus on day 4 ( $n = 5$ ). **c**, H3K27ac IF staining in the murine uterus on day 4. **d**, Pathway enrichment analysis of downregulated DEGs in the aging murine uterus. **e**, Heatmaps showing expression changes of selected genes in the human endometrium and murine uterus (aging versus young). **f**, GSEA of gene expression changes in the murine uterus (aging versus young) against aging-related downregulated DEGs in the human endometrium. **g**, H3K27ac IF staining in the murine uterus. **h**, Schematic diagram of the A485 injection. **i**, H3K27ac IF staining in the uterus on day 4. **j**, Implantation sites visualized by the blue dye and unimplanted embryos obtained in A485. **k**, The number of implantation sites on day 5. **l**, Cytokeratin IF staining in the uterus on day 4. **m**, Ki67 IHC and MUC1 IF staining in the uterus on day 4. **n**, PGR/ER $\alpha$  IHC staining in the uterus on day 4 ( $n = 3$ ). **o**, PGR/ER $\alpha$  protein

levels in the uterus on day 4. **p,q**, Relative mRNA levels of *Pgr* and *Esr1* (**p**) and *Ltf*, *Muc1*, *Hoxa10*, *Hand2* and *Ihh* (**q**) in the uterus on day 4 ( $n = 5$ ). **r**, The relative mRNA level of *Pgr* in uterine stromal cells on day 4 ( $n = 3$ ). **s**, The apoptosis rate of uterine stromal cells ( $n = 3$ ). **t**, Images of the uterus on the fifth day after decidualogenic stimulus. **u**, The H3K27ac level in the uterus on day 4 ( $n = 3$ ). **v**, H3K27ac IF staining in the uterus on day 4. **w**, PCA plot of uterine RNA-seq data from all groups of mice. Scale bar, 50  $\mu$ m (except **t**). Nuclei were stained with hematoxylin in IHC staining and with DAPI in IF staining. Statistical analysis was performed by two-sided unpaired Student's  $t$ -test or Mann–Whitney  $U$  rank-sum test. Data are presented as mean  $\pm$  s.d. All replicates were biological replicates. CON, control; FC, fold change; FDR, false discovery rate; ge, glandular epithelium; GSEA, gene set enrichment analysis; le, luminal epithelium; NES, normalized enrichment score; ns, not significant;  $P$ .adj, adjusted  $P$  value; PC, principal component; PCA, principal component analysis; s, stroma.



Lastly, we comprehensively compared transcriptional changes among aging, H3K27ac loss and PGR inhibition by an integrated analysis of all the RNA-seq data. Uterine samples in the aging, A485 and RU486 groups shared similar transcriptional signatures, which were distinct from the young and control groups (Fig. 5w). Inhibition of either H3K27ac or PGR would result in aging-like transcriptional changes (Extended Data Fig. 8a–f), dysregulating genes and pathways closely related to uterine receptivity (Extended Data Fig. 8g,h). Our findings suggest that eliminating H3K27ac resembles the aging process and has similar transcriptional effects as PGR inhibition, although some genes and pathways were regulated by H3K27ac only (Extended Data Fig. 8f,g). These results collectively demonstrate that H3K27ac can regulate genes and pathways related to endometrial receptivity by itself or via PGR (Supplementary Fig. 1).

## Discussion

In 1983, the association between AMA and potential adverse pregnancy outcomes was reported<sup>52</sup>. Fertility heavily declines with increasing reproductive age<sup>53–55</sup>, accompanied by elevated risks of certain diseases, including early miscarriages, late miscarriages, diabetes and chromosomal abnormalities<sup>3,5,56,57</sup>. Retrospective cohort studies have suggested that donor age is crucial to successful pregnancy in oocyte donation<sup>10,58</sup>. Unlike comprehensive studies focusing on the impact of aging-related abnormalities in oocytes and embryos, the effect of endometrial aging on pregnancy outcomes remains controversial<sup>9,11–13,59,60</sup>. These studies were limited by either small sample sizes or the interference of potential confounders. It is critical to understand the relationship between endometrial disorders and adverse pregnancy outcomes in middle-aged patients. To address this challenge, we characterized pregnancy outcomes of patients over and under 35 years of age who underwent PGT-A at our hospital. This PGT-A cohort presumably controlled the potential impacts of embryonic aneuploidy. We observed significantly lower pregnancy rates in the middle-aged group, implying that endometrial aging adversely affects pregnancy. Our in-house cohort study provides several advantages that support the reliability of our findings: (1) a large cohort ( $n = 1,149$ ) in the same reproductive center; (2) matched oocyte and endometrium age while using PGT-A to control the embryonic aneuploidy; and (3) exclusion of diseases and factors that could interfere with endometrial receptivity. Even though PGT-A cannot rule out a non-aneuploidy aging effect on embryos, our results still represent a concrete effort to confirm the endometrial factor contributing to aging-related infertility, as embryonic aneuploidy is the leading cause of AMA pregnancy loss<sup>61,62</sup>.

To further understand endometrial aging, we systematically characterized aging human endometrial epithelial and stromal cells at molecular, cellular and histological levels. We identified that H3K27ac loss is closely associated with aging-related transcriptional changes and PGR depletion. Using RNA-seq and CUT&Tag data, we determined H3K27ac targets and correlated aging-related H3K27ac loss to impaired endometrial receptivity. We confirmed H3K27ac as an upstream regulator of PGR because eliminating H3K27ac in young human endometrial stromal cells substantially reduced PGR. Moreover, H3K27ac and PGR exhibited correlated genomic occupancies, and their simultaneous depletion was prevalent in genes relevant to endometrial receptivity. We extended our investigation using an aging mouse model to validate initial observations. Inhibiting H3K27ac in the uterus of young mice induced aging-like phenotypes, including decreased PGR, extensive transcriptional changes, excessive epithelial proliferation, increased stromal apoptosis and impaired stromal decidualization, indicating defective uterine receptivity. We also compared transcriptional changes induced by H3K27ac and PGR inhibitors. H3K27ac inhibition resembled transcriptional changes caused by PGR inhibition but with hundreds of genes affected by H3K27ac loss only. Therefore, H3K27ac may function as a critical epigenetic regulator of uterine gene expression in mice through PGR-dependent and PGR-independent manners.

H3K27ac is a well-established chromatin marker of active enhancers and promoters. It is critical to reproductive events, such as zygotic genome activation and early embryonic development<sup>63–65</sup>. However, the association between H3K27ac and endometrial aging has not been clarified yet. In the present study, we identified H3K27ac loss as a hallmark of endometrial/uterine aging in humans and mice. Further studies are needed to elucidate the causal factors of aging-related H3K27ac loss. Acetyl-CoA is a substrate of histone acetyltransferases<sup>66</sup>. The consistent ACS5 expression in the endometrial epithelium throughout the menstrual cycle suggests the functional role of acyl-CoA synthesis<sup>67</sup>. In aging mice, acetyl-CoA declines in the brain<sup>68</sup>. Increasing acetyl-CoA in the brain may help maintain mitochondrial homeostasis and mitigate aging-related metabolic deficits in Alzheimer's disease<sup>68</sup>. We, thus, speculate that aging-related disruption in acetyl-CoA metabolism may lead to H3K27ac loss.

PGR dysfunction was previously identified in the aging murine uterus<sup>69</sup>. Our work contributes to determining and characterizing an upstream regulator of PGR. However, due to the lack of the region-specific inhibitor of H3K27ac, our conclusions about the impact of H3K27ac and PGR loss on endometrial receptivity have not been fully confirmed<sup>70</sup>. It has been reported that H3K27ac regulates chromatin state and affects the expression and binding of transcription factors<sup>71–73</sup>. We cannot distinguish the direct regulatory function of H3K27ac from its effects mediated through PGR. Whether H3K27ac could affect endometrial receptivity independent of PGR remains an open question. Moreover, H3K27ac is not the only epigenetic regulator of PGR and genes relevant to endometrial receptivity. For instance, the causal relationship between DNA methylation and reproductive aging was also reported in mice<sup>74</sup>. DNA methylation, RNA methylation and histone modifications may collectively regulate PGR and endometrial receptivity. The dynamic interactions and regulatory functions of these epigenetic factors are worthy of extra exploration in the future.

In the present study, we confirmed that endometrial aging is one of the critical factors leading to adverse pregnancy outcomes. We further elaborate on relationships among H3K27ac loss, PGR depletion and endometrial aging. H3K27ac extends beyond direct modulation of PGR expression to cooperatively interact with PGR in coordinating the transcriptional network of endometrial receptivity. Our work provides a new theoretical basis for the underlying mechanism of impaired endometrial receptivity in middle-aged patients. H3K27ac and PGR loss could serve as potential biomarkers and therapeutic targets for endometrial aging, potentially improving the fertility of middle-aged patients.

## Methods

### Clinical data collection

The current study was conducted at the Center for Reproductive Medicine of Peking University Third Hospital. A real-world retrospective PGT-A cohort study was performed to evaluate the effects of AMA on endometrial receptivity and pregnancy outcomes. Subfertile couples who were referred to the Center for Reproductive Medicine of Peking University Third Hospital for a PGT-A procedure from January 2018 to December 2022 were potentially eligible if they had at least one autologous euploid blastocyst (no mosaics) destined for frozen-thawed embryo transfer (FET). None of the participants had been diagnosed with uterine adhesion, immune system disease, hyperprolactinemia or thyroid dysfunction before the recruitment. Additional exclusion criteria were as follows: (1) couples either did not have a developed embryo for biopsy or did not have a euploid blastocyst for transfer; and (2) couples had any disease that would interfere with endometrial receptivity, including endometriosis, adenomyosis, fibroids, polyps and polycystic ovary syndrome. Single blastocyst FET was performed each time until a live birth or exhaustion of all euploid embryos occurred. Some patients experienced repeated transfers using surplus euploids. Reproductive outcomes were compared between patients who were

younger than 35 years of age or 35 years of age or older at their last transfer. Biochemical pregnancy was determined by a positive serum  $\beta$ -hCG test result. The clinical pregnancy was defined as an ultrasonographic visible gestational sac inside the uterine cavity, and ectopic pregnancy was defined as outside the uterus. Early pregnancy loss was defined as pregnancy loss that occurred during the first trimester. Live birth was defined as the delivery of any viable neonate with gestational age  $\geq 24$  weeks. The sex of the newborn was counted after delivery.

### Clinical sample collection

All endometrial samples were obtained from normally cycling patients undergoing endometrial biopsy in our center due to infertility combined with an uneven internal echo of the uterine cavity detected by transvaginal ultrasound. All patients of the well-characterized samples were normo-ovulatory, with regular cycles (21–35 d), and had not been on steroid hormone medications within 3 months before the sampling. The endometrium was collected 7–10 d after the serum luteinizing hormone (LH) peak, or the endometrium was paraffin embedded and stained with hematoxylin and eosin (H&E), and the mid-secretory phase was determined by two senior pathologists. Patients with any pathological findings that invade the endometrial cavity, as previously detected by transvaginal ultrasound, pelvic magnetic resonance imaging, endometrial biopsy or serum cancer antigen (CA) 125 determination, such as endometriosis, submucosal myomas, intramural myomas  $>4$  cm and hydrosalpinx, were further excluded. The definition of middle-aged patients in this study is older than 35 years of age. Specimens of patients aged 24–32 and 38–45 were eventually selected for tissue collection. The menstrual cycle was mainly categorized into proliferative, mid-secretory or other phases based on histopathologic criteria and were retrospectively assigned back to samples.

This study was approved by the Ethics Committee of Reproductive Medicine of the Peking University Third Hospital (no. 20195Z-067). All procedures were performed following the principles stated in the Declaration of Helsinki. Written informed consent was obtained from all patients.

### Human primary endometrial stromal cell isolation, culture and treatment

Endometrial tissues of young and middle-aged patients were rinsed with DPBS to remove mucus and blood contaminants and then minced into 8–10-mm<sup>3</sup> fragments. The remaining tissues were digested with collagenase I and DNase I for 1 h, and cell suspensions were filtered through 100- $\mu$ m and 40- $\mu$ m wire gauze in sequence to remove excess epithelial cells. The filtered cell suspension was centrifuged to collect stromal cells. Approximately  $8 \times 10^5$  viable stromal cells were seeded into six-well plates and cultured in phenol red-free DMEM/F-12 (Gibco) with 10% charcoal-stripped FBS (CS-FBS; Vistech). After 4 h, the culture medium was changed to remove the floating cells.

After being passaged once, isolated stromal cells were used to induce decidualization. When the cell density reached 50–60%, the medium was replaced by phenol red-free DMEM/F-12 with 1% CS-FBS supplemented with 10 nM estradiol (Sigma-Aldrich, 613967) and 1  $\mu$ M progesterone (Sigma-Aldrich, P0130) for different days.

### Animal feeding and treatments

This study involves the use of animals and was reviewed and approved by our institutional animal ethics committee (A2023030). The experiments adhere to the guidelines set by the committee and are conducted following the principles of the 3Rs (Replacement, Reduction and Refinement) to ensure the ethical treatment of animals in research. All efforts have been made to minimize animal suffering and to use the minimum number of animals necessary to achieve the scientific objectives of the study.

Eight-week-old and 10-month-old C57BL/6J mice were acquired from Beijing Vital River Laboratory Animal Technology. All mice were

kept in a controlled environment with a 12-h light/dark cycle, a room temperature of 20–25 °C and humidity of 55%  $\pm$  10% and had access to food and water at all times.

Female mice were mated with male mice, and the day of detection of vaginal plug was considered day 1 of the pregnancy. On day 3 of the pregnancy, mice in the case group received injections of 5  $\mu$ l of 100  $\mu$ M A485 (Selleck Chemicals, S8740) or RU486 (Selleck Chemicals, S2606) on each side of the uterine horn, whereas mice in the control group were given 5  $\mu$ l of DPBS on each side of the uterine horn. On day 4 of the pregnancy, endometrial samples were obtained for molecular testing. On day 5 of the pregnancy, implantation sites were identified with an intravenous injection of Chicago blue dye solution (Sigma-Aldrich, C8679), and the number of implantation sites, marked by distinct blue bands, was recorded.

### Western blotting

Western blotting was performed as previously described<sup>75</sup>. Samples were homogenized in the lysis buffer, followed by the separation of proteins on a 12% SDS-PAGE gel. After this, the proteins were transferred to PVDF membranes (Millipore) and blocked with 5% non-fat dry milk. Specific primary and secondary antibodies were then incubated on the membranes in sequence. Antibodies against H3K27ac, IGFBP1, PGR, ER $\alpha$ , p300, FoxO1, HOXA10 and HAND2 were used. GAPDH served as control. Detailed information for antibodies is provided in Supplementary Table 5.

### qRT-PCR

Total RNA was extracted from uterine tissues or cells using TRIzol reagent (Thermo Fisher Scientific). cDNA was made by HiScript II Q RT SuperMix for qPCR (+gDNA wiper) (Vazyme Biotech, R323-01). qRT-PCR was performed using SsoFast EvaGreen Supermix (Bio-Rad, 172-5201) on a QuantStudio 12K Flex (Applied Biosystems). Each PCR experiment was repeated at least three times, and relative expression levels were determined by the  $\Delta$ CT method with normalization to GAPDH. All PCR primers are listed in Supplementary Table 6.

### Immunostaining

Human endometrial and mouse uterine tissues were fixed in 4% paraformaldehyde. Five-micrometer paraffin-embedded sections were used for immunohistochemistry staining. Rehydrated sections were microwaved in sodium citrate buffer for 20 min to repair antigens and then blocked with 0.5% BSA-PBS for 1 h. After this, the primary antibodies PGR, ER $\alpha$  and Ki67 were incubated at 4 °C overnight. Signals were visualized by horseradish peroxidase (HRP)-conjugated secondary antibodies. In immunofluorescence experiments, paraffin-embedded sections and cells were incubated with H3K27ac, MUC1 and phalloidin primary antibodies. Signals were visualized by secondary antibodies labeled with Alexa Fluor 488 (anti-rabbit; Invitrogen), and the cell nuclei were stained with DAPI. Detailed information for antibodies is provided in Supplementary Table 5.

### Co-IP

The human endometrium was used for co-IP. Diluted p300 and IgG antibodies were added to magnetic beads, which were then fully suspended and incubated in a flip mixer for 30 min at room temperature, followed by 2 h at 4 °C. After rinsing the magnetic beads (MCE, HY-K0202) with PBST, samples were added and incubated overnight at 4 °C in a flip mixer. The magnetic beads were then separated and resolved by SDS-PAGE. Magnetic beads were isolated and redissolved by 1 $\times$  SDS-PAGE loading buffer, and subsequent immunoblot experiments were performed using antibodies against PGR and ER $\alpha$ .

### RNA isolation and library preparation

Total RNA was extracted from human endometrium and mouse uteri using TRIzol reagent (Invitrogen) according to the manufac-

turer's protocol. RNA purity and quantification were evaluated using a NanoDrop 2000 spectrophotometer (Thermo Fisher Scientific). RNA integrity was checked using an Agilent 2100 Bioanalyzer (Agilent Technologies). Then, the libraries were constructed using the VAHTS Universal V6 RNA-seq Library Prep Kit according to the manufacturer's instructions. The transcriptome sequencing and analysis were conducted by OE Biotech Co., Ltd. Each group was performed with at least three biological replicates.

### RNA-seq and analysis

The libraries were sequenced on an Illumina NovaSeq 6000 platform, and 150-bp paired-end reads were generated. Approximately 50 million raw reads were generated for each sample. Raw reads in FASTQ format were first processed using fastp<sup>76</sup>, and low-quality reads were removed to obtain clean reads. Approximately 48 million clean reads were retained for each sample. Clean reads were then mapped to the reference genome using HISAT2 (ref. 77). Human reference genome hg38 was used for the human data, and mouse reference genome mm39 was used for the murine data. Read counts of each gene were obtained by HTSeq-count<sup>78</sup>. Differential expression analysis was performed by DESeq2 (ref. 79). DEGs were determined by adjusted  $P < 0.05$  and absolute  $\log_2$  fold change  $> 1$ . The enrichment analysis was performed by Metascape<sup>80</sup>. Aging-related DEGs in the human endometrium were compared to published chromatin immunoprecipitation sequencing (ChIP-seq) data of histone modifications<sup>81–86</sup>.

### CUT&Tag library construction

Cell nuclei extracted from the mid-secretory endometrium of young and middle-aged groups were used for CUT&Tag assay after being isolated using a cell nuclear isolation kit (Bioyou, S2201-10). CUT&Tag assay was performed using a Hyperactive Universal CUT&Tag Assay Kit for Illumina (Vazyme Biotech, TD903) according to the manufacturer's instructions<sup>87</sup>. Initially, concanavalin A-coated magnetic beads (ConA beads) were added to resuspended cell nuclei and incubated at room temperature to bind the cell nuclei. Cell membrane permeabilization was achieved using the non-ionic detergent Digitonin. The cell nuclei were then bound by ConA beads. Subsequently, primary antibodies for H3K27ac and PGR, along with secondary antibodies and the Hyperactive pA-Tn5 Transposase, were incubated with the nuclei. The Hyperactive pA-Tn5 Transposase precisely cleaved the DNA fragments bound to the target proteins. The cut DNA fragments were ligated with P5 and P7 adaptors by Tn5 transposase, and the libraries were amplified by PCR using the P5 and P7 primers. The purified PCR products were assessed using the Agilent 2100 Bioanalyzer. Finally, the libraries were sequenced on the Illumina NovaSeq 6000 platform, generating 150-bp paired-end reads for subsequent analysis. Each group was performed with three biological replicates.

### CUT&Tag analysis

The raw sequence data were first trimmed by fastp<sup>76</sup> to obtain clean reads. Clean reads were aligned to the human reference genome hg38 using Bowtie 2 (ref. 88). Peak calling was performed by MACS2 with the 'narrowPeak' parameter<sup>89</sup>. Normalization was performed with the RPGC method. Peak annotation was performed by ChIPseeker<sup>90</sup>. The motif analysis was conducted by Homer<sup>91</sup>. Differentially binding peaks were determined by DiffBind<sup>92</sup>, with adjusted  $P < 0.05$  and absolute  $\log_2$  fold change  $> 0.75$ .

### Statistics and reproducibility

For the cohort study, categorical variables were shown in ratio and percentage, and differences between groups were compared by Fisher's exact test or chi-square test, as specified in the legend. Continuous variables were reported as mean  $\pm$  s.d. and compared by the Mann-Whitney  $U$  rank-sum test owing to the non-normality of data. All experiments were repeated at least three times. Data are presented as mean  $\pm$  s.d. in

a combo chart with columns and scatter plots. Statistical analysis was performed by two-sided unpaired Student's  $t$ -test or Mann-Whitney  $U$  rank-sum test (when data did not follow a normal distribution). Statistical analysis and visualization were performed using Prism for Windows (version 9.5.1; GraphPad Software). A two-tailed  $P$  value less than 0.05 was considered statistically significant. No statistical methods were used to predetermine sample sizes, but our sample sizes are similar to those reported in previous publications<sup>93–95</sup>.

No data were excluded from the analyses. Data collection and analysis were not performed blinded to the conditions of the experiments.

### Reporting summary

Further information on research design is available in the Nature Portfolio Reporting Summary linked to this article.

### Data availability

All data supporting the study's findings are provided in the Source Data and Supplementary Information. Human RNA-seq and CUT&Tag data have been uploaded to the Genome Sequence Archive (accession number [HRA007501](https://www.genome.gov/HRA007501)). Murine RNA-seq data have been uploaded to the Genome Sequence Archive (accession number [CRA022502](https://www.genome.gov/CRA022502)). BED files of CUT&Tag data have been uploaded to the Open Archive for Miscellaneous Data (accession number OMIX008964). The human reference genome hg38 can be accessed in the National Center for Biotechnology Information (NCBI) ([https://ftp.ncbi.nlm.nih.gov/genomes/all/GCF/000/001/405/GCF\\_000001405.39\\_GRCh38.p13/](https://ftp.ncbi.nlm.nih.gov/genomes/all/GCF/000/001/405/GCF_000001405.39_GRCh38.p13/)). The mouse reference genome mm39 can be accessed in the NCBI ([https://ftp.ncbi.nlm.nih.gov/genomes/all/GCF/000/001/635/GCF\\_000001635.27\\_GRCm39/](https://ftp.ncbi.nlm.nih.gov/genomes/all/GCF/000/001/635/GCF_000001635.27_GRCm39/)). Source data are provided with this paper.

### References

- Heffner, L. J. Advanced maternal age—how old is too old? *N. Engl. J. Med.* **351**, 1927–1929 (2004).
- Sauer, M. V. Reproduction at an advanced maternal age and maternal health. *Fertil. Steril.* **103**, 1136–1143 (2015).
- Frick, A. P. Advanced maternal age and adverse pregnancy outcomes. *Best Pract. Res. Clin. Obstet. Gynaecol.* **70**, 92–100 (2021).
- Beaujouan, É. & Toulemon, L. European countries with delayed childbearing are not those with lower fertility. *Genus* **77**, 2 (2021).
- Magnus, M. C., Wilcox, A. J., Morken, N.-H., Weinberg, C. R. & Håberg, S. E. Role of maternal age and pregnancy history in risk of miscarriage: prospective register based study. *BMJ* **364**, l869 (2019).
- Khalil, A., Syngelaki, A., Maiz, N., Zinevich, Y. & Nicolaidis, K. H. Maternal age and adverse pregnancy outcome: a cohort study. *Ultrasound Obstet. Gynecol.* **42**, 634–643 (2013).
- Jacobsson, B., Ladfors, L. & Milsom, I. Advanced maternal age and adverse perinatal outcome. *Obstet. Gynecol.* **104**, 727–733 (2004).
- Lean, S. C., Derricott, H., Jones, R. L. & Heazell, A. E. Advanced maternal age and adverse pregnancy outcomes: a systematic review and meta-analysis. *PLoS ONE* **12**, e0186287 (2017).
- Balmaceda, J. P. et al. Implantation: oocyte donation in humans: a model to study the effect of age on embryo implantation rate. *Hum. Reprod.* **9**, 2160–2163 (1994).
- Cohen, M. A., Lindheim, S. R. & Sauer, M. V. Donor age is paramount to success in oocyte donation. *Hum. Reprod.* **14**, 2755–2758 (1999).
- Meldrum, D. R. Female reproductive aging—ovarian and uterine factors. *Fertil. Steril.* **59**, 1–5 (1993).
- Yaron, Y. et al. Oocyte donation in Israel: a study of 1001 initiated treatment cycles. *Hum. Reprod.* **13**, 1819–1824 (1998).
- Pathare, A. D. et al. Endometrial receptivity in women of advanced age: an underrated factor in infertility. *Hum. Reprod. Update* **29**, 773–793 (2023).

14. Sharma, A. & Kumar, P. Understanding implantation window, a crucial phenomenon. *J. Hum. Reprod. Sci.* **5**, 2–6 (2012).
15. Massimiani, M. et al. Molecular signaling regulating endometrium–blastocyst crosstalk. *Int. J. Mol. Sci.* **21**, 23 (2019).
16. Cha, J., Sun, X. & Dey, S. K. Mechanisms of implantation: strategies for successful pregnancy. *Nat. Med.* **18**, 1754–1767 (2012).
17. Yoshinaga, K. Uterine receptivity for blastocyst implantation. *Ann. N Y Acad. Sci.* **541**, 424–431 (1988).
18. Enciso, M. et al. The precise determination of the window of implantation significantly improves ART outcomes. *Sci. Rep.* **11**, 13420 (2021).
19. Lessey, B. A. & Young, S. L. What exactly is endometrial receptivity? *Fertil. Steril.* **111**, 611–617 (2019).
20. Wang, W. et al. Single-cell transcriptomic atlas of the human endometrium during the menstrual cycle. *Nat. Med.* **26**, 1644–1653 (2020).
21. Norwitz, E. R., Schust, D. J. & Fisher, S. J. Implantation and the survival of early pregnancy. *N. Engl. J. Med.* **345**, 1400–1408 (2001).
22. Fazleabas, A. T. & Strakova, Z. Endometrial function: cell specific changes in the uterine environment. *Mol. Cell. Endocrinol.* **186**, 143–147 (2002).
23. Su, R.-W. & Fazleabas, A. T. in *Regulation of Implantation and Establishment of Pregnancy in Mammals: Tribute to 45 Year Anniversary of Roger V. Short's 'Maternal Recognition of Pregnancy'* (eds Geisert, R. D. & Bazer, F. W.) 189–213 (Springer, 2015).
24. Liu, H., Huang, X., Mor, G. & Liao, A. Epigenetic modifications working in the decidualization and endometrial receptivity. *Cell. Mol. Life Sci.* **77**, 2091–2101 (2020).
25. Wang, H. & Dey, S. K. Roadmap to embryo implantation: clues from mouse models. *Nat. Rev. Genet.* **7**, 185–199 (2006).
26. Kato, N. et al. Reciprocal changes of H3K27ac and H3K27me3 at the promoter regions of the critical genes for endometrial decidualization. *Epigenomics* **10**, 1243–1257 (2018).
27. Grimaldi, G. et al. Down-regulation of the histone methyltransferase EZH2 contributes to the epigenetic programming of decidualizing human endometrial stromal cells. *Mol. Endocrinol.* **25**, 1892–1903 (2011).
28. Tamura, I. et al. The distal upstream region of insulin-like growth factor-binding protein-1 enhances its expression in endometrial stromal cells during decidualization. *J. Biol. Chem.* **293**, 5270–5280 (2018).
29. Harper, M. J. The implantation window. *Baillieres Clin. Obstet. Gynaecol.* **6**, 351–371 (1992).
30. Newman, A. M. et al. Determining cell type abundance and expression from bulk tissues with digital cytometry. *Nat. Biotechnol.* **37**, 773–782 (2019).
31. Deng, N. et al. H3K27me3 timely dictates uterine epithelial transcriptome remodeling and thus transformation essential for normal embryo implantation. *Cell Death Differ.* **31**, 1018–1028 (2024).
32. Zhang, B. et al. A dynamic H3K27ac signature identifies VEGFA-stimulated endothelial enhancers and requires EP300 activity. *Genome Res.* **23**, 917–927 (2013).
33. Zhang, T., Zhang, Z., Dong, Q., Xiong, J. & Zhu, B. Histone H3K27 acetylation is dispensable for enhancer activity in mouse embryonic stem cells. *Genome Biol.* **21**, 45 (2020).
34. Li, Q. et al. WNT4 acts downstream of BMP2 and functions via  $\beta$ -catenin signaling pathway to regulate human endometrial stromal cell differentiation. *Endocrinology* **154**, 446–457 (2013).
35. Rider, V. et al. WINGLESS (WNT) signaling is a progesterone target for rat uterine stromal cell proliferation. *J. Endocrinol.* **229**, 197–207 (2016).
36. Lee, K. Y. et al. Bmp2 is critical for the murine uterine decidual response. *Mol. Cell. Biol.* **27**, 5468–5478 (2007).
37. Nallasamy, S. et al. *Msx* homeobox genes act downstream of BMP2 to regulate endometrial decidualization in mice and in humans. *Endocrinology* **160**, 1631–1644 (2019).
38. Iwahashi, M., Muragaki, Y., Ooshima, A., Yamoto, M. & Nakano, R. Alterations in distribution and composition of the extracellular matrix during decidualization of the human endometrium. *Reproduction* **108**, 147–155 (1996).
39. Song, Y. et al. Activated Hippo/Yes-associated protein pathway promotes cell proliferation and anti-apoptosis in endometrial stromal cells of endometriosis. *J. Clin. Endocrinol. Metab.* **101**, 1552–1561 (2016).
40. Dunlap, K. A. et al. Postnatal deletion of *Wnt7a* inhibits uterine gland morphogenesis and compromises adult fertility in mice. *Biol. Reprod.* **85**, 386–396 (2011).
41. Tepekoy, F., Akkoyunlu, G. & Demir, R. The role of Wnt signaling members in the uterus and embryo during pre-implantation and implantation. *J. Assist. Reprod. Genet.* **32**, 337–346 (2015).
42. Favaro, R., Abrahamsohn, P. A. & Zorn, M. T. in *The Guide to Investigation of Mouse Pregnancy* 125–142 (Elsevier, 2014).
43. Zhu, H., Jiang, Y., Pan, Y., Shi, L. & Zhang, S. Human menstrual blood-derived stem cells promote the repair of impaired endometrial stromal cells by activating the p38 MAPK and AKT signaling pathways. *Reprod. Biol.* **18**, 274–281 (2018).
44. Chen, L. J. et al. Single xenotransplant of rat brown adipose tissue prolonged the ovarian lifespan of aging mice by improving follicle survival. *Aging Cell* **18**, e13024 (2019).
45. Franks, L. & Payne, J. The influence of age on reproductive capacity in C57BL mice. *Reproduction* **21**, 563–565 (1970).
46. Liu, B. et al. BDNF promotes mouse follicular development and reverses ovarian aging by promoting cell proliferation. *J. Ovarian Res.* **16**, 83 (2023).
47. Das, S. K. Cell cycle regulatory control for uterine stromal cell decidualization in implantation. *Reproduction* **137**, 889–899 (2009).
48. Wang, Q. et al. *Wnt6* is essential for stromal cell proliferation during decidualization in mice. *Biol. Reprod.* **88**, 5 (2013).
49. Nagashima, T. et al. Bmpr2 is required for postimplantation uterine function and pregnancy maintenance. *J. Clin. Invest.* **123**, 2539–2550 (2013).
50. Okada, H., Tsuzuki, T. & Murata, H. Decidualization of the human endometrium. *Reprod. Med. Biol.* **17**, 220–227 (2018).
51. Ramathal, C. Y., Bagchi, I. C., Taylor, R. N. & Bagchi, M. K. Endometrial decidualization: of mice and men. *Semin. Reprod. Med.* **28**, 17–26 (2010).
52. Naeye, R. L. Maternal age, obstetric complications, and the outcome of pregnancy. *Obstet. Gynecol.* **61**, 210–216 (1983).
53. Garcia, D., Brazal, S., Rodriguez, A., Prat, A. & Vassena, R. Knowledge of age-related fertility decline in women: a systematic review. *Eur. J. Obstet. Gynecol. Reprod. Biol.* **230**, 109–118 (2018).
54. American College of Obstetricians and Gynecologists Committee on Gynecologic Practice and Practice Committee. Female age-related fertility decline. Committee Opinion No. 589. *Fertil. Steril.* **101**, 633–634 (2014).
55. Yaron, Y. et al. Endometrial receptivity: the age-related decline in pregnancy rates and the effect of ovarian function. *Fertil. Steril.* **60**, 314–318 (1993).
56. Schimmel, M. S. et al. The effects of maternal age and parity on maternal and neonatal outcome. *Arch. Gynecol. Obstet.* **291**, 793–798 (2015).
57. Zhang, C., Yan, L. & Qiao, J. Effect of advanced parental age on pregnancy outcome and offspring health. *J. Assist. Reprod. Genet.* **39**, 1969–1986 (2022).

58. Hogan, R. G. et al. Oocyte donor age has a significant impact on oocyte recipients' cumulative live-birth rate: a population-based cohort study. *Fertil. Steril.* **112**, 724–730 (2019).
59. Mirkin, S. et al. Factors associated with an optimal pregnancy outcome in an oocyte donation program. *J. Assist. Reprod. Genet.* **20**, 400–408 (2003).
60. Wang, Y. A., Farquhar, C. & Sullivan, E. A. Donor age is a major determinant of success of oocyte donation/recipient programme. *Hum. Reprod.* **27**, 118–125 (2012).
61. Cimadomo, D. et al. Opening the black box: why do euploid blastocysts fail to implant? A systematic review and meta-analysis. *Hum. Reprod. Update* **29**, 570–633 (2023).
62. Vitagliano, A., Paffoni, A. & Viganò, P. Does maternal age affect assisted reproduction technology success rates after euploid embryo transfer? A systematic review and meta-analysis. *Fertil. Steril.* **120**, 251–265 (2023).
63. Wu, K. et al. Dynamics of histone acetylation during human early embryogenesis. *Cell Discov.* **9**, 29 (2023).
64. Wang, M., Chen, Z. & Zhang, Y. CBP/p300 and HDAC activities regulate H3K27 acetylation dynamics and zygotic genome activation in mouse preimplantation embryos. *EMBO J.* **41**, e112012 (2022).
65. Li, J. et al. Metabolic control of histone acetylation for precise and timely regulation of minor ZGA in early mammalian embryos. *Cell Discov.* **8**, 96 (2022).
66. Bradshaw, P. C. Acetyl-CoA metabolism and histone acetylation in the regulation of aging and lifespan. *Antioxidants* **10**, 572 (2021).
67. Gassler, N. et al. Expression of acyl-CoA synthetase 5 in human endometrium and in endometrioid adenocarcinomas. *Histopathology* **47**, 501–507 (2005).
68. Currais, A. et al. Elevating acetyl-CoA levels reduces aspects of brain aging. *eLife* **8**, e47866 (2019).
69. Woods, L. et al. Decidualisation and placentation defects are a major cause of age-related reproductive decline. *Nat. Commun.* **8**, 352 (2017).
70. Tie, F. et al. CBP-mediated acetylation of histone H3 lysine 27 antagonizes *Drosophila* Polycomb silencing. *Development* **136**, 3131–3141 (2009).
71. Zhao, J., Li, X., Guo, M., Yu, J. & Yan, C. The common stress responsive transcription factor ATF3 binds genomic sites enriched with p300 and H3K27ac for transcriptional regulation. *BMC Genomics* **17**, 335 (2016).
72. Beacon, T. H. et al. The dynamic broad epigenetic (H3K4me3, H3K27ac) domain as a mark of essential genes. *Clin. Epigenetics* **13**, 138 (2021).
73. Zhang, S. et al. H3K27ac nucleosomes facilitate HMGN1 localization at regulatory sites to modulate chromatin binding of transcription factors. *Commun. Biol.* **5**, 159 (2022).
74. Woods, L. et al. Epigenetic changes occur at decidualisation genes as a function of reproductive ageing in mice. *Development* **147**, dev185629 (2020).
75. Zhao, W. et al. Progesterone activates the histone lactylation–Hif1 $\alpha$ –glycolysis feedback loop to promote decidualization. *Endocrinology* **165**, bqad169 (2023).
76. Chen, S., Zhou, Y., Chen, Y. & Gu, J. fastp: an ultra-fast all-in-one FASTQ preprocessor. *Bioinformatics* **34**, i884–i890 (2018).
77. Kim, D., Langmead, B. & Salzberg, S. L. HISAT: a fast spliced aligner with low memory requirements. *Nat. Methods* **12**, 357–360 (2015).
78. Anders, S., Pyl, P. T. & Huber, W. HTSeq—a Python framework to work with high-throughput sequencing data. *Bioinformatics* **31**, 166–169 (2015).
79. Love, M. I., Huber, W. & Anders, S. Moderated estimation of fold change and dispersion for RNA-seq data with DESeq2. *Genome Biol.* **15**, 550 (2014).
80. Zhou, Y. et al. Metascape provides a biologist-oriented resource for the analysis of systems-level datasets. *Nat. Commun.* **10**, 1523 (2019).
81. Kim, S. W. et al. Chromatin and transcriptional signatures for Nodal signaling during endoderm formation in hESCs. *Dev. Biol.* **357**, 492–504 (2011).
82. Tamura, I. et al. Genome-wide analysis of histone modifications in human endometrial stromal cells. *Mol. Endocrinol.* **28**, 1656–1669 (2014).
83. Lister, R. et al. Human DNA methylomes at base resolution show widespread epigenomic differences. *Nature* **462**, 315–322 (2009).
84. Bernstein, B. E. et al. The NIH roadmap epigenomics mapping consortium. *Nat. Biotechnol.* **28**, 1045–1048 (2010).
85. Guenther, M. G. et al. Chromatin structure and gene expression programs of human embryonic and induced pluripotent stem cells. *Cell Stem Cell* **7**, 249–257 (2010).
86. Vermeulen, M. et al. Quantitative interaction proteomics and genome-wide profiling of epigenetic histone marks and their readers. *Cell* **142**, 967–980 (2010).
87. Kaya-Okur, H. S. et al. CUT&Tag for efficient epigenomic profiling of small samples and single cells. *Nat. Commun.* **10**, 1930 (2019).
88. Langmead, B. & Salzberg, S. L. Fast gapped-read alignment with Bowtie 2. *Nat. Methods* **9**, 357–359 (2012).
89. Zhang, Y. et al. Model-based analysis of ChIP-Seq (MACS). *Genome Biol.* **9**, R137 (2008).
90. Yu, G., Wang, L.-G. & He, Q.-Y. ChIPseeker: an R/Bioconductor package for ChIP peak annotation, comparison and visualization. *Bioinformatics* **31**, 2382–2383 (2015).
91. Heinz, S. et al. Simple combinations of lineage-determining transcription factors prime cis-regulatory elements required for macrophage and B cell identities. *Mol. Cell* **38**, 576–589 (2010).
92. Ross-Innes, C. S. et al. Differential oestrogen receptor binding is associated with clinical outcome in breast cancer. *Nature* **481**, 389–393 (2012).
93. Chen, X. et al. Small extracellular vesicles from young plasma reverse age-related functional declines by improving mitochondrial energy metabolism. *Nat. Aging* **4**, 814–838 (2024).
94. Huang, P. et al. SOX4 facilitates PGR protein stability and FOXO1 expression conducive for human endometrial decidualization. *eLife* **11**, e72073 (2022).
95. Tang, Y. et al. P38 $\alpha$  MAPK is a gatekeeper of uterine progesterone responsiveness at peri-implantation via Ube3c-mediated PGR degradation. *Proc. Natl Acad. Sci. USA* **119**, e2206000119 (2022).

## Acknowledgements

This work was supported by the National Key Research and Development Project of China (2021YFC2700303 and 2022YFC2702500), the National Natural Science Foundation of China (81925013, 82288102, 82225019, 82192873, 82301888 and 82271699), the Key Clinical Projects of Peking University Third Hospital (BYSYZD2023028), the Beijing Nova Program (20220484073), the Special Project on Capital Clinical Diagnosis and Treatment Technology Research and Transformation Application (Z211100002921054) and Frontiers Medical Center, Tianfu Jincheng Laboratory Foundation (TFJCP120250032). We want to thank all the patients and staff of the Center for Reproductive Medicine, Department of Obstetrics and Gynecology, Peking University Third Hospital for their contributions. We thank CapitalBio Corporation for technical assistance.

## Author contributions

Concept and design: R.L., H.P., Y.Y. and Y.W. Acquisition, analysis or interpretation of data: M.C. and Y.W. Drafting of the paper: Y.W., P.Z. and H.S. The experiments were performed and data were analyzed by, and critical revision of the paper for important intellectual content was performed by, H.S., X.L., M.C., Z.Y., X.C., B.L., T.P., C.X., Z.H. and Y.D. Obtained funding: R.L., H.P., Y.Y. and Y.W. Administrative, technical

or material support: R.L., H.P. and Y.Y. Supervision: R.L. All authors approved the final version for submission.

### Competing interests

The authors declare no competing interests.

### Additional information

**Extended data** is available for this paper at <https://doi.org/10.1038/s43587-025-00859-5>.

**Supplementary information** The online version contains supplementary material available at <https://doi.org/10.1038/s43587-025-00859-5>.

**Correspondence and requests for materials** should be addressed to Yang Yu, Heng Pan or Rong Li.

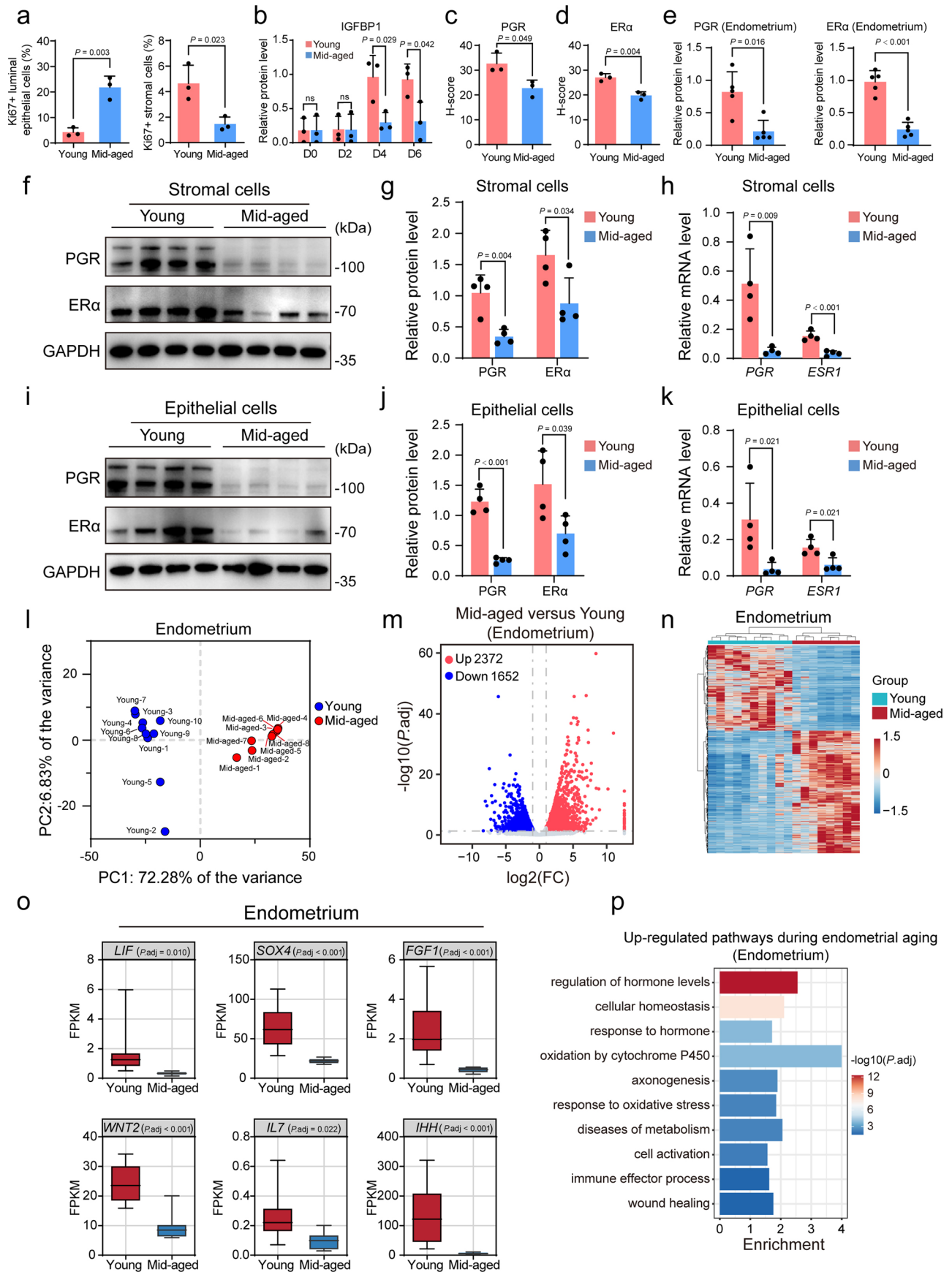
**Peer review information** *Nature Aging* thanks Francesco Demayo and the other, anonymous, reviewer(s) for their contribution to the peer review of this work.

**Reprints and permissions information** is available at [www.nature.com/reprints](http://www.nature.com/reprints).

**Publisher's note** Springer Nature remains neutral with regard to jurisdictional claims in published maps and institutional affiliations.

**Open Access** This article is licensed under a Creative Commons Attribution-NonCommercial-NoDerivatives 4.0 International License, which permits any non-commercial use, sharing, distribution and reproduction in any medium or format, as long as you give appropriate credit to the original author(s) and the source, provide a link to the Creative Commons licence, and indicate if you modified the licensed material. You do not have permission under this licence to share adapted material derived from this article or parts of it. The images or other third party material in this article are included in the article's Creative Commons licence, unless indicated otherwise in a credit line to the material. If material is not included in the article's Creative Commons licence and your intended use is not permitted by statutory regulation or exceeds the permitted use, you will need to obtain permission directly from the copyright holder. To view a copy of this licence, visit <http://creativecommons.org/licenses/by-nc-nd/4.0/>.

© The Author(s) 2025

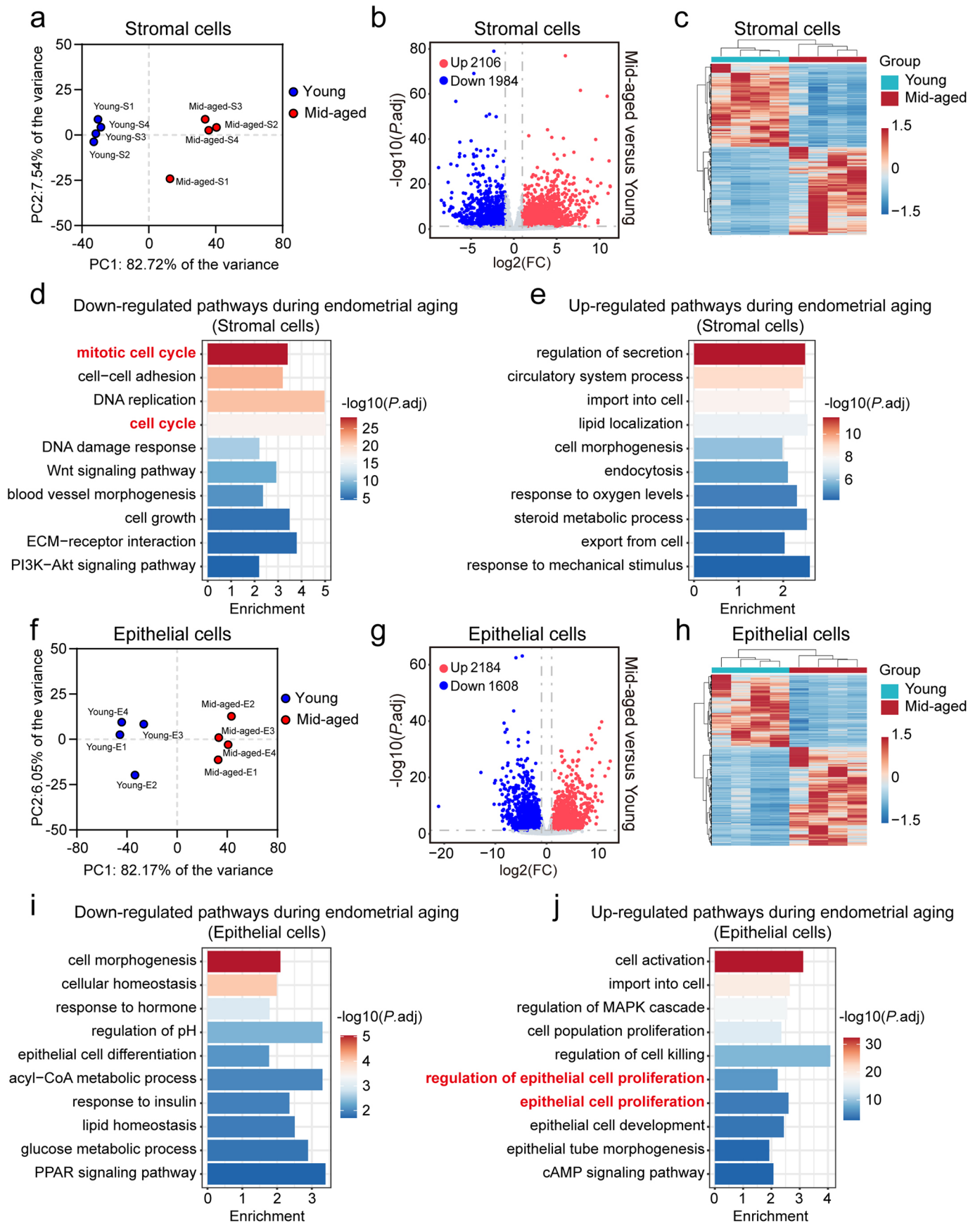


Extended Data Fig. 1 | See next page for caption.

**Extended Data Fig. 1 | The mid-secretory endometrium exhibits different phenotypes and gene expression between young and middle-aged patients.**

**a**, The percentage of Ki67-positive cells in endometrial luminal epithelial and stromal cells in the mid-secretory phase ( $n = 3$ ). **b**, Relative protein levels of IGFBP1 in human endometrial stromal cells during induced decidualization ( $n = 3$ ). **c,d**, Histochemical scoring assessment (H-score) of PGR and ER $\alpha$  in the mid-secretory endometrium ( $n = 3$ ). **e**, Relative protein levels of PGR and ER $\alpha$  in the mid-secretory endometrium ( $n = 5$ ). **f,g**, Protein levels of PGR and ER $\alpha$  in human mid-secretory endometrial stromal cells ( $n = 4$ ). **h**, Relative mRNA levels of *PGR* and *ESR1* in human mid-secretory endometrial stromal cells ( $n = 4$ ). **i,j**, Protein levels of PGR and ER $\alpha$  in human mid-secretory endometrial epithelial cells ( $n = 4$ ). **k**, Relative mRNA levels of *PGR* and *ESR1* in human mid-secretory endometrial epithelial cells ( $n = 4$ ). **l**, PCA plot of human mid-secretory endometrial RNA-seq data. **m**, Volcano plot illustrating gene expression changes

between the young and aging mid-secretory endometrium ( $|\log_2FC| > 1$ ,  $P_{adj} < 0.05$ ). **n**, Heatmap showing gene expression of differentially expressed genes (DEGs) between the young and aging mid-secretory endometrium. **o**, FPKM of *LIF*, *SOX4*, *FGF1*, *WNT2*, *IL7*, *IHH* in the human mid-secretory endometrium ( $n = 10$  and  $n = 8$  for the young and middle-aged groups, respectively). The adjusted  $P$  value was determined by DESeq2. Whiskers represent upper quartile + 1.5 interquartile range (IQR) and lower quartile - 1.5 IQR. **p**, Pathway enrichment analysis of upregulated DEGs in the aging mid-secretory endometrium. Statistical analysis was performed by two-sided unpaired Student's  $t$ -test or Mann-Whitney  $U$  rank-sum test. Data are presented as mean  $\pm$  s.d. All replicates were biological replicates. FC, fold change; mid-aged, middle-aged; ns, not significant;  $P_{adj}$ , adjusted  $P$  value; PC, principal component; PCA, principal component analysis.

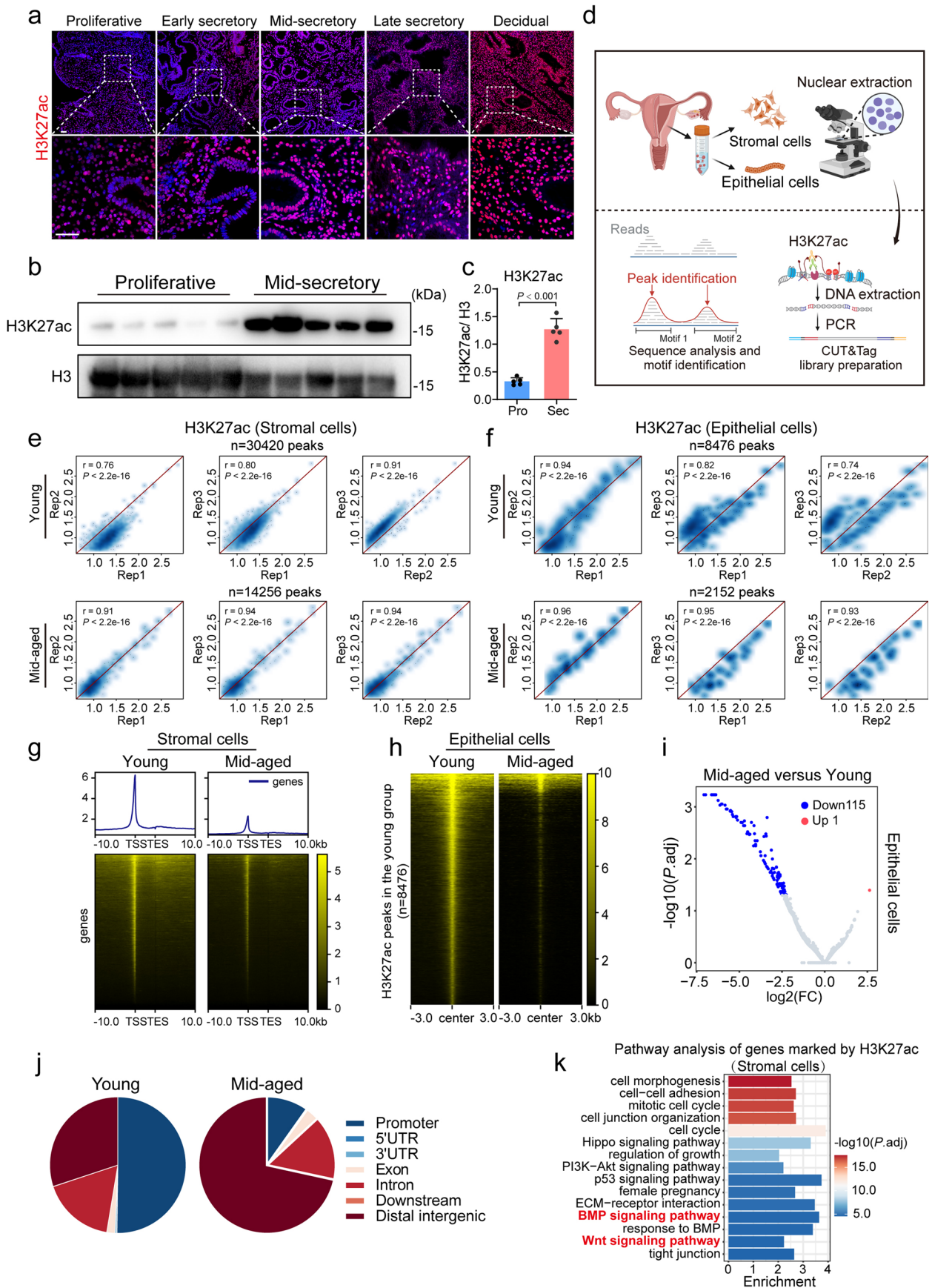


Extended Data Fig. 2 | See next page for caption.

**Extended Data Fig. 2 | Mid-secretory endometrial stromal and epithelial cells show different gene expression between young and middle-aged patients.**

**a**, PCA plot of RNA-seq data of mid-secretory endometrial stromal cells ( $n = 4$ ). **b**, Volcano plot illustrating gene expression changes between young and aging mid-secretory endometrial stromal cells ( $|\log_2FC| > 1, P_{adj} < 0.05$ ). **c**, Heatmap showing gene expression of DEGs between young and aging mid-secretory endometrial stromal cells. **d**, Pathway enrichment analysis of downregulated DEGs in aging mid-secretory endometrial stromal cells. **e**, Pathway enrichment analysis of upregulated DEGs in aging mid-secretory endometrial stromal cells. **f**, PCA plot of RNA-seq data

of mid-secretory endometrial epithelial cells ( $n = 4$ ). **g**, Volcano plot illustrating gene expression changes between young and aging mid-secretory endometrial epithelial cells ( $|\log_2FC| > 1, P_{adj} < 0.05$ ). **h**, Heatmap showing gene expression of DEGs between young and aging mid-secretory endometrial epithelial cells. **i**, Pathway enrichment analysis of downregulated DEGs in aging mid-secretory endometrial epithelial cells. **j**, Pathway enrichment analysis of upregulated DEGs in aging mid-secretory endometrial epithelial cells. All replicates were biological replicates. FC, fold change; mid-aged, middle-aged;  $P_{adj}$ , adjusted  $P$  value; PC, principal component; PCA, principal component analysis.

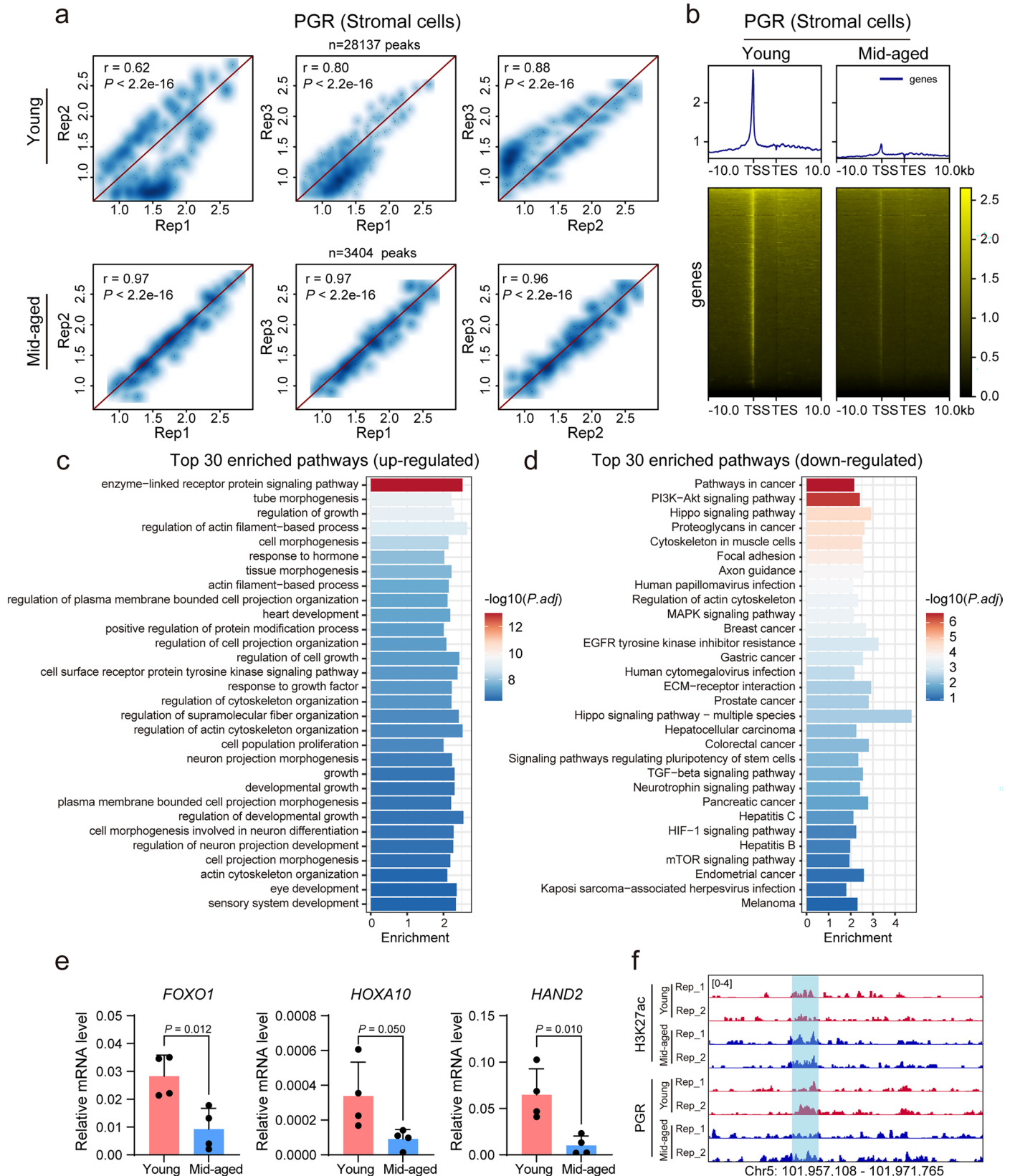


Extended Data Fig. 3 | See next page for caption.

**Extended Data Fig. 3 | Genome-wide H3K27ac signals in mid-secretory endometrial stromal and epithelial cells of young and middle-aged patients.**

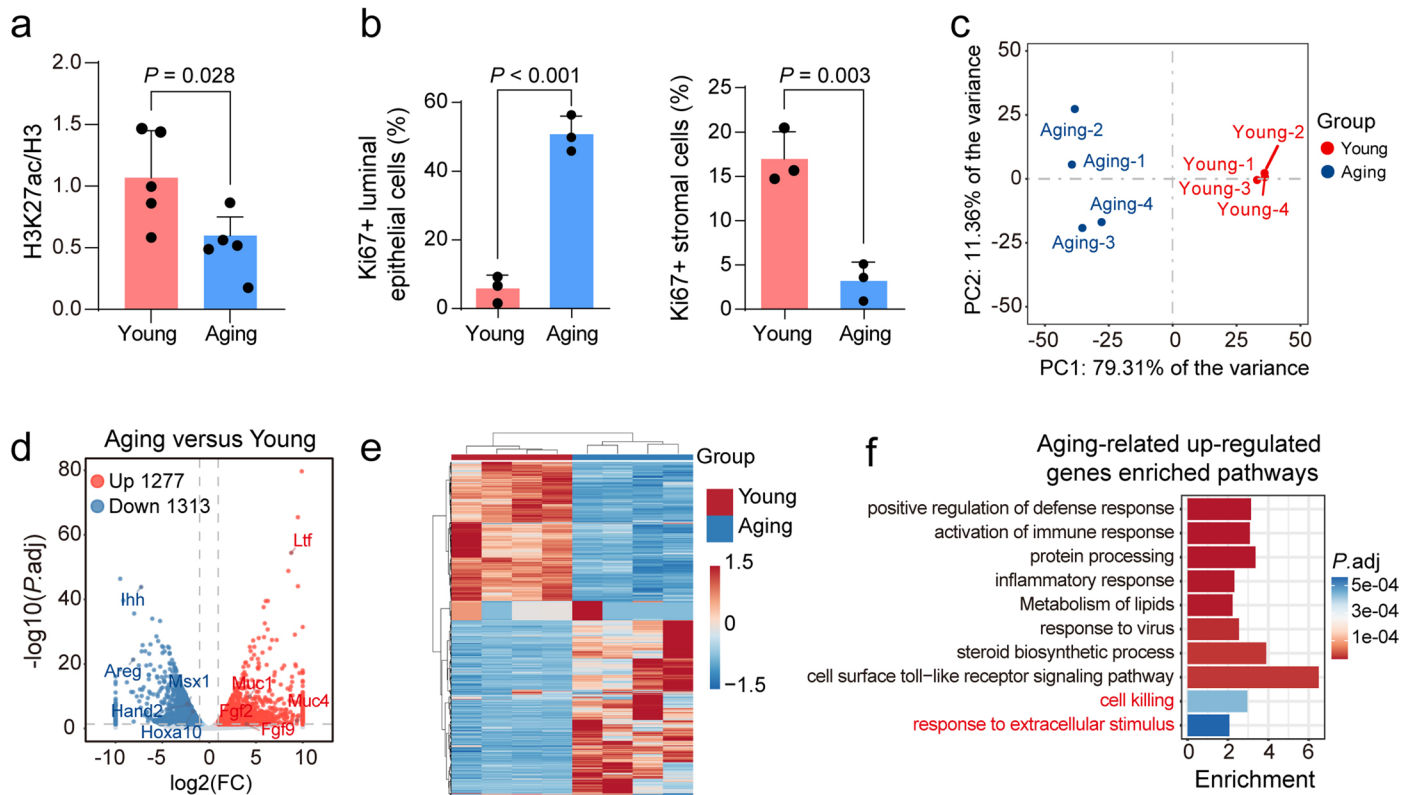
**a**, H3K27ac immunofluorescence (IF) staining in the endometrium of different hormonal stages. Scale bar: 50  $\mu\text{m}$ . **b,c**, H3K27ac in the human proliferative and mid-secretory endometrium ( $n = 5$ ). Statistical analysis was performed by two-sided unpaired Student's  $t$ -test. Data are presented as mean  $\pm$  s.d. **d**, Schematic design of H3K27ac CUT&Tag in mid-secretory endometrial stromal and epithelial cells. **e,f**, Consistent H3K27ac signals between biological replicates ( $n = 3$ ). **g**, Heatmaps of the H3K27ac signal in human mid-secretory endometrial stromal cells around gene bodies. **h**, Heatmaps of the H3K27ac signal in human

mid-secretory endometrial epithelial cells at H3K27ac peaks in the young group. **i**, Volcano plot illustrating H3K27ac differences between young and aging mid-secretory endometrial epithelial cells. Red and blue points represent peaks that gain and lose H3K27ac in aging epithelial cells. **j**, The genomic distribution of H3K27ac peaks in human mid-secretory endometrial epithelial cells. **k**, Pathway enrichment analysis of genes marked by H3K27ac in young mid-secretory endometrial stromal cells. All replicates were biological replicates. FC, fold change; mid-aged, middle-aged;  $P_{\text{adj}}$ , adjusted  $P$  value; PC, principal component; PCA, principal component analysis; Pro, proliferative phase; Sec, secretory phase; TES, transcription end site; UTR, untranslated region.



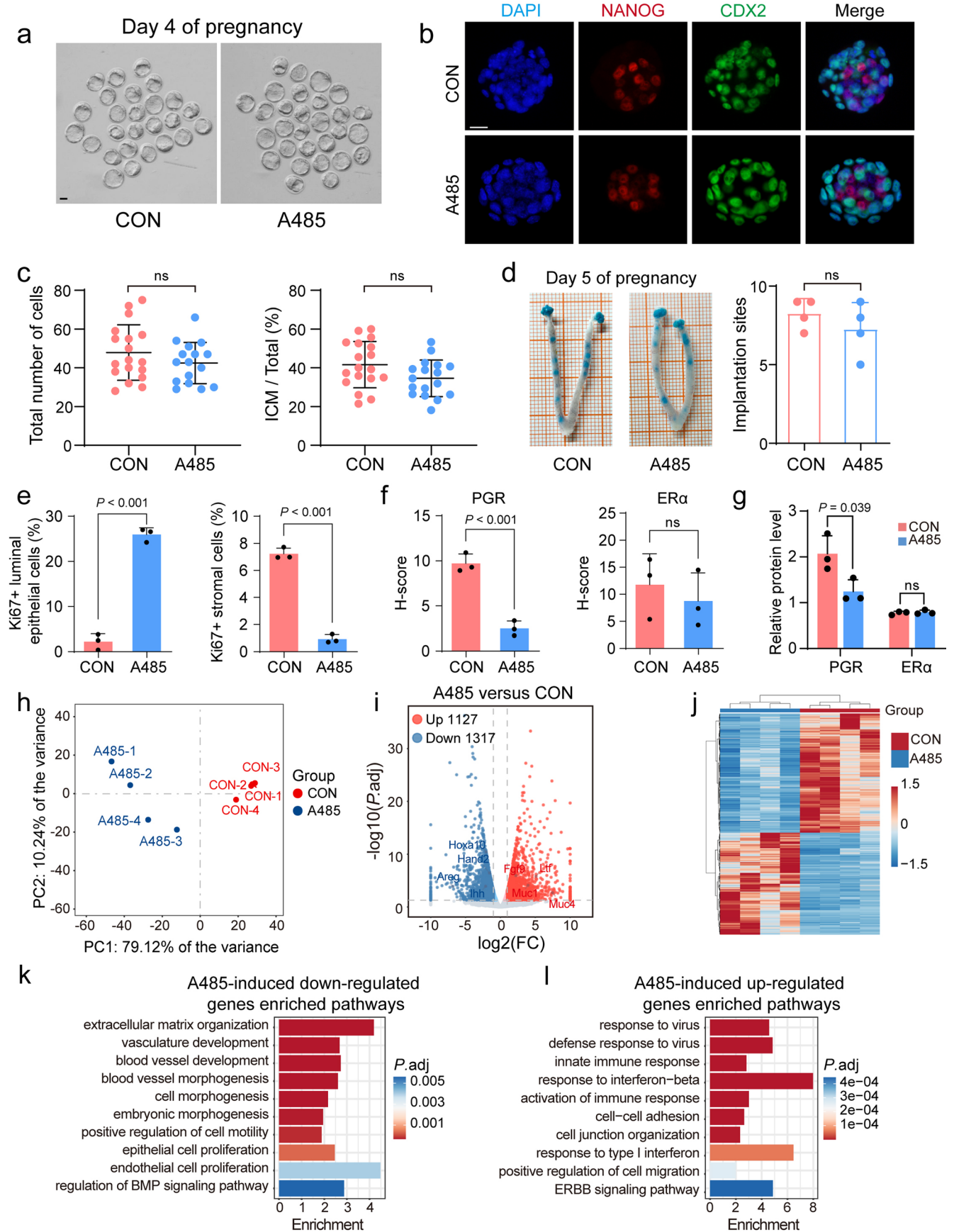
**Extended Data Fig. 4 | Genome-wide PGR signals in mid-secretory endometrial stromal cells of young and middle-aged patients. a**, Consistent PGR signals between biological replicates ( $n = 3$ ). **b**, Heatmaps of the PGR signal in human mid-secretory stromal cells around gene bodies. **c**, Pathway enrichment analysis of genes with PGR gain in aging mid-secretory endometrial stromal cells. **d**, Pathway enrichment analysis of genes with PGR loss in aging mid-secretory endometrial stromal cells. **e**, Relative mRNA levels of *FOXO1*, *HOXA10* and *HAND2*

in human mid-secretory endometrial stromal cells ( $n = 4$ ). Statistical analysis was performed by two-sided unpaired Student's *t*-test. Data are presented as mean  $\pm$  s.d. **f**, H3K27ac and PGR signals in mid-secretory endometrial stromal cells at the selected region. hg38 coordinates are shown. All replicates were biological replicates. *P*.adj, adjusted *P* value; mid-aged, middle-aged; TES, transcription site.



**Extended Data Fig. 5 | The uterus exhibits different gene expression between young and aging mice.** **a**, H3K27ac in the murine uterus ( $n = 5$ ). **b**, The percentage of Ki67-positive cells in uterine epithelial and stromal cells ( $n = 3$ ). **c**, PCA Plot of murine uterine RNA-seq data ( $n = 4$ ). **d**, Volcano plot illustrating gene expression changes between young and aging mice ( $|\log_2FC| > 1$ ,  $P_{adj} < 0.05$ ). **e**, Heatmap showing gene expression of DEGs between the young and aging murine uterus.

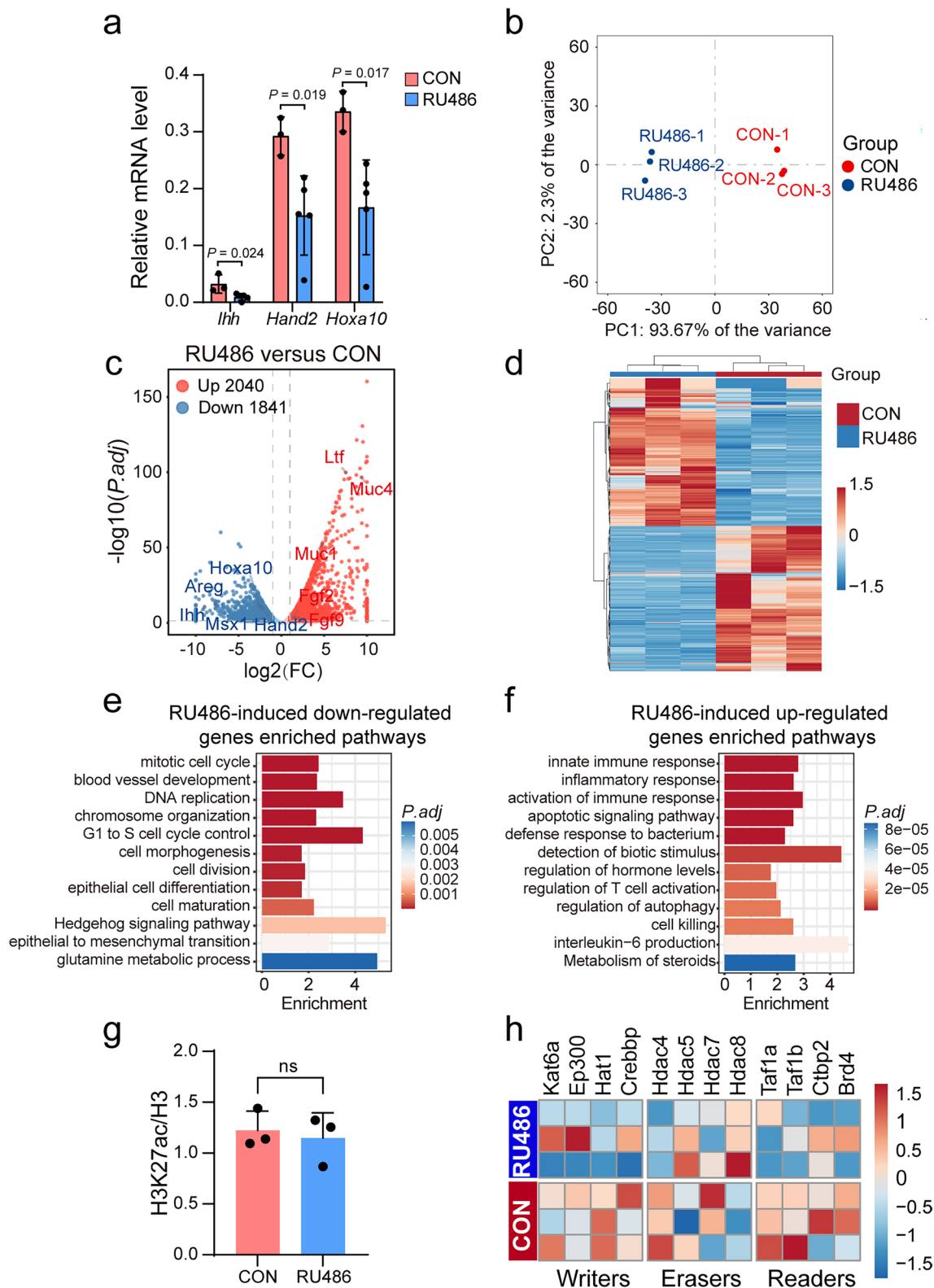
**f**, Pathway enrichment analysis of upregulated DEGs in the aging murine uterus. In **a** and **b**, statistical analysis was performed by two-sided Student's *t*-test or Mann-Whitney *U* rank-sum test. Data are presented as mean  $\pm$  s.d. All replicates were biological replicates. FC, fold change;  $P_{adj}$ , adjusted *P* value; PC, principal component; PCA, principal component analysis.



Extended Data Fig. 6 | See next page for caption.

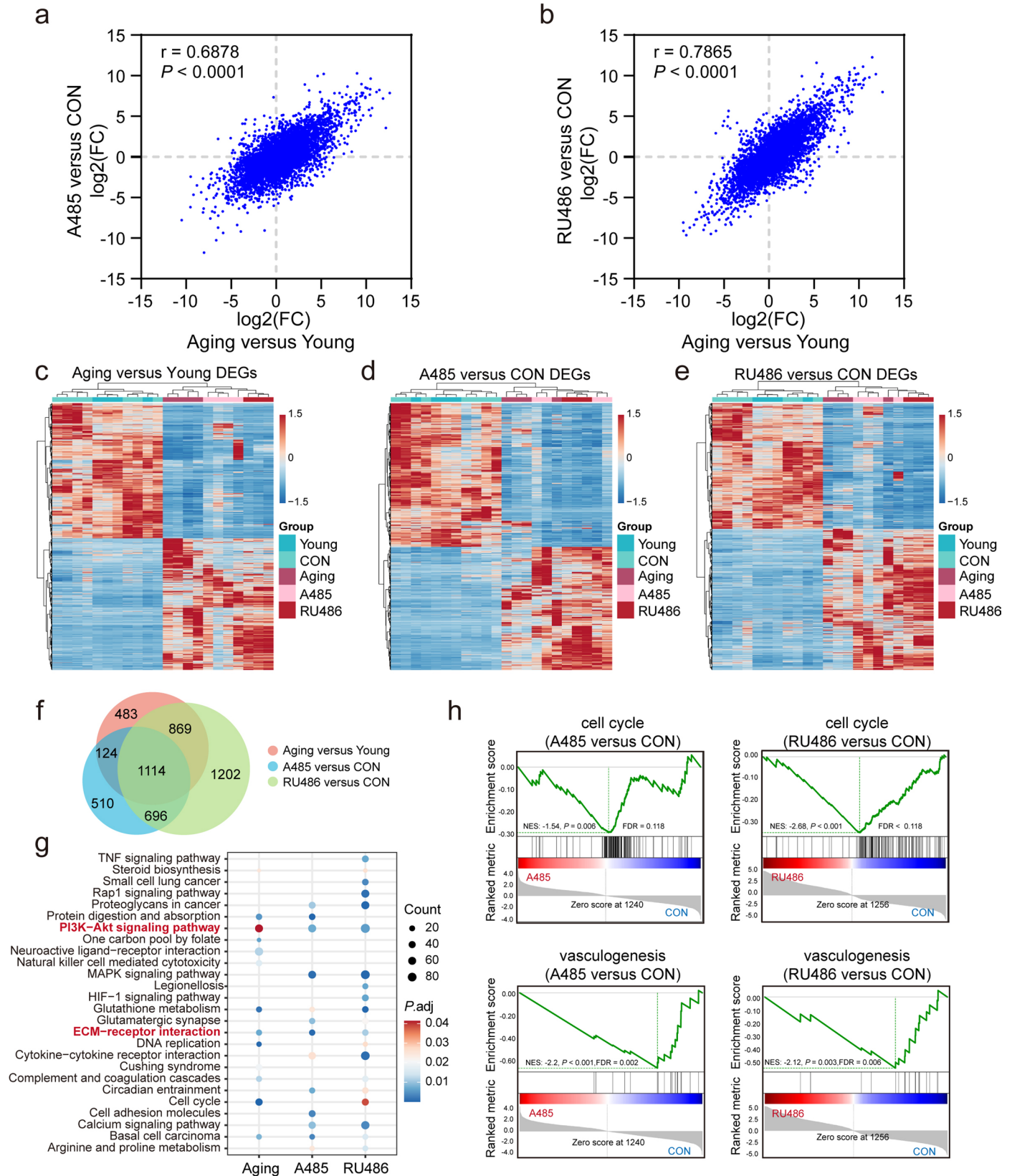
**Extended Data Fig. 6 | Eliminating H3K27ac impairs murine uterine receptivity.** **a**, Blastocysts retrieved from the CON and A485 groups. **b**, NANOG (inner cell mass marker) and CDX2 (trophectoderm marker) IF staining in blastocysts. **c**, The number of cells per blastocyst and the percentage of inner cell mass cells. **d**, Blastocysts were transplanted into sham pregnant mice and the number of implantation sites were measured on day 5. **e**, The percentage of Ki67-positive cells in uterine epithelial and stromal cells ( $n = 3$ ). **f**, The H-score of PGR and ER $\alpha$  in the uterus on day 4 ( $n = 3$ ). **g**, Relative protein levels of PGR and ER $\alpha$  in the uterus on day 4 ( $n = 3$ ). **h**, PCA plot of murine uterine RNA-seq data ( $n = 4$ ).

**i**, Volcano plot illustrating gene expression changes between the CON and A485 murine uterus ( $|\log_2FC| > 1$ ,  $P_{adj} < 0.05$ ). **j**, Heatmap showing gene expression of DEGs between the CON and A485 murine uterus. **k**, Pathway enrichment analysis of downregulated DEGs in the A485 murine uterus. **l**, Pathway enrichment analysis of upregulated DEGs in the A485 murine uterus. Statistical analysis was performed by two-sided unpaired Student's  $t$ -test or Mann–Whitney  $U$  rank-sum test. Data are presented as mean  $\pm$  s.d. All replicates were biological replicates. CON, control; FC, fold change; ns, not significant;  $P_{adj}$ , adjusted  $P$  value; PC, principal component; PCA, principal component analysis.



**Extended Data Fig. 7 | Inhibiting PGR induces murine uterine transcriptional changes without affecting H3K27ac. a**, Relative mRNA levels of *Ihh*, *Hand2* and *Hoxa10* in the uterus on day 4 ( $n = 3$  and  $n = 5$  for the CON and RU486 groups, respectively). **b**, PCA plot of murine uterine RNA-seq data ( $n = 3$ ). **c**, Volcano plot illustrating gene expression changes between the CON and RU486 murine uterus ( $|\log_2FC| > 1$ ,  $P_{adj} < 0.05$ ). **d**, Heatmap showing gene expression of DEGs between the CON and RU486 murine uterus. **e**, Pathway enrichment analysis of downregulated DEGs in the RU486 murine uterus. **f**, Pathway enrichment analysis

of upregulated DEGs in the RU486 murine uterus. **g**, H3K27ac in the murine uterus ( $n = 3$ ). **h**, Heatmaps showing gene expression of H3K27ac writers, erasers and readers in the murine uterus. In **a** and **g**, statistical analysis was performed by two-sided unpaired Student's  $t$ -test. Data are presented as mean  $\pm$  s.d. All replicates were biological replicates. CON, control; FC, fold change; ns, not significant;  $P_{adj}$ , adjusted  $P$  value; PC, principal component; PCA, principal component analysis.



**Extended Data Fig. 8 | Inhibiting H3K27ac or PGR resembles aging-related transcriptomic changes in the murine uterus. a**, Consistent gene expression changes between A485/CON and Aging/Young. **b**, Consistent gene expression changes between RU486/CON and Aging/Young. **c**, Heatmap showing gene expression of DEGs between the young and aging murine uterus. **d**, Heatmap showing gene expression of DEGs between the CON and A485 murine uterus.

**e**, Heatmap showing gene expression of DEGs between the CON and RU486 murine uterus. **f**, Venn diagram illustrating the overlap among different groups of DEGs. **g**, KEGG enrichment analysis of different groups of DEGs. **h**, GSEA of gene expression changes in the murine uterus (A485 or RU486 versus CON) against the cell cycle and vasculogenesis gene sets. CON, control; FC, fold change;  $P_{adj}$ , adjusted  $P$  value.

## Reporting Summary

Nature Portfolio wishes to improve the reproducibility of the work that we publish. This form provides structure for consistency and transparency in reporting. For further information on Nature Portfolio policies, see our [Editorial Policies](#) and the [Editorial Policy Checklist](#).

### Statistics

For all statistical analyses, confirm that the following items are present in the figure legend, table legend, main text, or Methods section.

- |                                     |  |
|-------------------------------------|--|
| n/a                                 | Confirmed  |
| <input type="checkbox"/>            | <input checked="" type="checkbox"/> The exact sample size ( $n$ ) for each experimental group/condition, given as a discrete number and unit of measurement  |
| <input type="checkbox"/>            | <input checked="" type="checkbox"/> A statement on whether measurements were taken from distinct samples or whether the same sample was measured repeatedly  |
| <input type="checkbox"/>            | <input checked="" type="checkbox"/> The statistical test(s) used AND whether they are one- or two-sided<br><i>Only common tests should be described solely by name; describe more complex techniques in the Methods section.</i>   |
| <input type="checkbox"/>            | <input checked="" type="checkbox"/> A description of all covariates tested   |
| <input type="checkbox"/>            | <input checked="" type="checkbox"/> A description of any assumptions or corrections, such as tests of normality and adjustment for multiple comparisons  |
| <input type="checkbox"/>            | <input checked="" type="checkbox"/> A full description of the statistical parameters including central tendency (e.g. means) or other basic estimates (e.g. regression coefficient) AND variation (e.g. standard deviation) or associated estimates of uncertainty (e.g. confidence intervals) |
| <input type="checkbox"/>            | <input checked="" type="checkbox"/> For null hypothesis testing, the test statistic (e.g. $F$ , $t$ , $r$ ) with confidence intervals, effect sizes, degrees of freedom and $P$ value noted<br><i>Give <math>P</math> values as exact values whenever suitable.</i>                            |
| <input checked="" type="checkbox"/> | <input type="checkbox"/> For Bayesian analysis, information on the choice of priors and Markov chain Monte Carlo settings  |
| <input checked="" type="checkbox"/> | <input type="checkbox"/> For hierarchical and complex designs, identification of the appropriate level for tests and full reporting of outcomes  |
| <input checked="" type="checkbox"/> | <input type="checkbox"/> Estimates of effect sizes (e.g. Cohen's $d$ , Pearson's $r$ ), indicating how they were calculated  |

*Our web collection on [statistics for biologists](#) contains articles on many of the points above.*

### Software and code

Policy information about [availability of computer code](#)

**Data collection** Immunofluorescence results were obtained by ZEISS LSM710-LASER SCANNING CONFOCAL. The H&E and immunohistochemistry results were collected by NIS-Elements 3.2. CUT&Tag and RNA-seq data were collected by the Illumina NovaSeq 6000 platform.

**Data analysis** fastp (version 0.20.1), HISAT2 (version 2.1.0), HTSeq-count (version 0.11.2), DESeq2 (version 1.22.2), python (version 3.10.8), Bowtie2 (version 2.5.1), MACS2 (version 2.2.9.1), ChIPseeker (version 1.36.0), Homer (version 4.11), R (version 4.3.1), Diffbind (version 3.12.0), GraphPad Prism (version 9.5.1), GSEA (version 4.3.2).

For manuscripts utilizing custom algorithms or software that are central to the research but not yet described in published literature, software must be made available to editors and reviewers. We strongly encourage code deposition in a community repository (e.g. GitHub). See the Nature Portfolio [guidelines for submitting code & software](#) for further information.

### Data

Policy information about [availability of data](#)

All manuscripts must include a [data availability statement](#). This statement should provide the following information, where applicable:

- Accession codes, unique identifiers, or web links for publicly available datasets
- A description of any restrictions on data availability
- For clinical datasets or third party data, please ensure that the statement adheres to our [policy](#)

Human RNA-seq and CUT&Tag data have been uploaded to the Genome Sequence Archive (accession number: HRA007501).

Murine RNA-seq data have been uploaded to the Genome Sequence Archive (accession number: CRA022502).

BED files of CUT&Tag data have been uploaded to the Open Archive for Miscellaneous Data (accession number: OMIX008964).

The human reference genome hg38 can be accessed in NCBI ([https://ftp.ncbi.nlm.nih.gov/genomes/all/GCF/000/001/405/GCF\\_000001405.39\\_GRCh38.p13/](https://ftp.ncbi.nlm.nih.gov/genomes/all/GCF/000/001/405/GCF_000001405.39_GRCh38.p13/)).

The mouse reference genome mm39 can be accessed in NCBI ([https://ftp.ncbi.nlm.nih.gov/genomes/all/GCF/000/001/635/GCF\\_000001635.27\\_GRCm39/](https://ftp.ncbi.nlm.nih.gov/genomes/all/GCF/000/001/635/GCF_000001635.27_GRCm39/)).

## Research involving human participants, their data, or biological material

Policy information about studies with [human participants or human data](#). See also policy information about [sex, gender \(identity/presentation\), and sexual orientation](#) and [race, ethnicity and racism](#).

Reporting on sex and gender	Endometrial samples of both young and aging women.
Reporting on race, ethnicity, or other socially relevant groupings	No socially relevant groupings were included.
Population characteristics	Human endometrial tissues were collected from women aged 24-32 and 38-45. Endometrial tissues in the proliferative, mid-secretory, or other phases of the menstrual cycle were collected. The phases were determined based on histopathologic criteria and were retrospectively assigned to samples.
Recruitment	All participants were norm-ovulatory, with the regular cycle (21-35 days), and had not been on the steroid hormone medication within 3 months before sampling. Patients with any pathological finding invading the endometrial cavity previously detected by transvaginal ultrasound, such as adenomyosis, submucosal myomas or intramural myomas > 4 cm, and hydrosalpinx, were further excluded.
Ethics oversight	This study was approved by the Ethics Committee of Reproductive Medicine, Peking University Third Hospital (No. 20195Z-067).

Note that full information on the approval of the study protocol must also be provided in the manuscript.

## Field-specific reporting

Please select the one below that is the best fit for your research. If you are not sure, read the appropriate sections before making your selection.

Life sciences  Behavioural & social sciences  Ecological, evolutionary & environmental sciences

For a reference copy of the document with all sections, see [nature.com/documents/nr-reporting-summary-flat.pdf](https://www.nature.com/documents/nr-reporting-summary-flat.pdf)

## Life sciences study design

All studies must disclose on these points even when the disclosure is negative.

Sample size	No statistical methods were used to pre-determine sample sizes, but our sample sizes were similar to those reported in previous publications (PMCID: PMC11186790, PMC8923662, PMC9371708).
Data exclusions	No data were excluded in this study.
Replication	Each experiment was repeated at least three times and all attempts at replication were successful.
Randomization	We ensured comparable baseline characteristics between selected samples of the young and aging groups in both human and mice. Human and murine samples were evenly and randomly assigned to the control and treatment groups.
Blinding	Blinding design was not necessary in this study since the sequencing and evaluation processes were equally for all the human endometrial samples and murine uterine samples.

## Behavioural & social sciences study design

All studies must disclose on these points even when the disclosure is negative.

Study description	n/a
Research sample	n/a
Sampling strategy	n/a
Data collection	n/a
Timing	n/a

Data exclusions	n/a
Non-participation	n/a
Randomization	n/a

## Ecological, evolutionary & environmental sciences study design

All studies must disclose on these points even when the disclosure is negative.

Study description	n/a
Research sample	n/a
Sampling strategy	n/a
Data collection	n/a
Timing and spatial scale	n/a
Data exclusions	n/a
Reproducibility	n/a
Randomization	n/a
Blinding	n/a

Did the study involve field work?  Yes  No

## Reporting for specific materials, systems and methods

We require information from authors about some types of materials, experimental systems and methods used in many studies. Here, indicate whether each material, system or method listed is relevant to your study. If you are not sure if a list item applies to your research, read the appropriate section before selecting a response.

### Materials & experimental systems

### Methods

- n/a | Involved in the study
- Antibodies
  - Eukaryotic cell lines
  - Palaeontology and archaeology
  - Animals and other organisms
  - Clinical data
  - Dual use research of concern
  - Plants

- n/a | Involved in the study
- ChIP-seq
  - Flow cytometry
  - MRI-based neuroimaging

### Antibodies

Antibodies used

Progesterone Receptor A/B (D8Q2J) XP® Rabbit mAb, Cell signaling Technology, USA, Cat#8757T, 1:1000 dilution.  
 Acetyl-Histone H3 (Lys27) (D5E4) XP® Rabbit mAb, Cell signaling Technology, USA, Cat#8173S, 1:1000 dilution.  
 IGFBP1 (D4E9T) XP® Rabbit mAb, Cell signaling Technology, USA, Cat#31025T, 1:1000 dilution.  
 Anti-Estrogen Receptor alpha antibody [E115] - CHIP Grade, Abcam, UK, Cat#ab32063, 1:1000 dilution.  
 Anti-Histone H3 Marker and CHIP Grade, Abcam, UK, Cat#ab1791, 1:1000 dilution.  
 Anti-Estrogen Receptor alpha antibody, Abcam, UK, Cat#ab75635, 1:200 dilution.  
 Rabbit monoclonal [EPR1023] to MUC1, Abcam, UK, Cat#ab109185, 1:200 dilution.  
 Mouse monoclonal [6C5] to GAPDH - Loading Control, Abcam, UK, Cat#ab8245, 1:1000 dilution.  
 Rabbit polyclonal to Ki67, Abcam, UK, Cat#ab15580, 1:200 dilution.  
 Rabbit monoclonal [EPR2764Y] to CDX2, Abcam, UK, Cat#ab76541, 1:50 dilution.  
 Nanog Antibody (A-11), SANTA CRUZ, USA, Cat#sc-374001, 1:50 dilution.  
 Phalloidin-iFluor 555 Abcam, UK, Cat#ab176756, 1:200 dilution.  
 Rabbit monoclonal [EPR1619Y] to Cytokeratin 7 - Cytoskeleton Marker, UK, Cat#ab68459, 1:200 dilution.  
 p300 (D8Z4E) Rabbit mAb, Cell signaling Technology, USA, Cat#86377S, 1:1000 dilution.  
 FoxO1 (C29H4) Rabbit mAb, Cell signaling Technology, USA, Cat#2880T, 1:1000 dilution.

Rabbit monoclonal [EPR27317-76] to HOXA10, Abcam, UK, Cat#ab308516, 1:1000 dilution.  
 Rabbit monoclonal [EPR19451] to HAND2, Abcam, UK, Cat#ab200040, 1:1000 dilution.  
 Invitrogen Goat anti-Rabbit IgG (H+L) Highly Cross-Adsorbed Secondary Antibody, Alexa Fluor Plus 555, Thermo Fisher Scientific, USA, Cat#A32732, 1:1000 dilution.

## Validation

Progesterone Receptor <https://www.cellsignal.com/products/primary-antibodies/progesterone-receptor-a-b-d8q2j-xp-rabbit-mab/8757>  
 Acetyl-Histone H3 (Lys27) <https://www.cellsignal.com/products/primary-antibodies/acetyl-histone-h3-lys27-d5e4-xp-rabbit-mab/8173>  
 IGFBP1 <https://www.cellsignal.com/products/primary-antibodies/igfbp1-d4e9t-xp-rabbit-mab/31025>  
 Anti-Estrogen Receptor alpha <https://www.abcam.cn/products/primary-antibodies/estrogen-receptor-alpha-antibody-e115-chip-grade-ab32063.html>  
 Anti-Histone H3 <https://www.abcam.cn/products/primary-antibodies/histone-h3-antibody-nuclear-marker-and-chip-grade-ab1791.html>  
 Anti-Estrogen Receptor alpha antibody <https://www.abcam.cn/products/primary-antibodies/estrogen-receptor-alpha-antibody-ab75635.html>  
 MUC1 <https://www.abcam.cn/products/primary-antibodies/muc1-antibody-epr1023-ab109185.html>  
 GAPDH <https://www.abcam.cn/products/primary-antibodies/gapdh-antibody-6c5-loading-control-ab8245.html>  
 Ki67 <https://www.abcam.cn/products/primary-antibodies/ki67-antibody-ab15580.html>  
 CDX2 <https://www.abcam.cn/products/primary-antibodies/cdx2-antibody-epr2764y-ab76541.html>  
 Nanog <https://www.scbt.com/p/nanog-antibody-a-11>  
 Phalloidin-iFluor 555 <https://www.abcam.cn/products/assay-kits/phalloidin-ifluor-555-reagent-ab176756.html>  
 Cytokeratin 7 <https://www.abcam.cn/products/primary-antibodies/cytokeratin-7-antibody-epr1619y-cytoskeleton-marker-ab68459.html>  
 p300 <https://www.cellsignal.com/products/primary-antibodies/p300-d8z4e-rabbit-mab/86377>  
 FoxO1 <https://www.cellsignal.com/products/primary-antibodies/foxo1-c29h4-rabbit-mab/2880>  
 HOXA10 <https://www.abcam.cn/products/primary-antibodies/hoxa10-antibody-epr27317-76-ab308516.html>  
 HAND2 <https://www.abcam.cn/products/primary-antibodies/hand2-antibody-epr19451-ab200040.html>  
 Goat anti-Rabbit IgG (H+L) Highly Cross-Adsorbed Secondary Antibody <https://www.thermofisher.cn/cn/zh/antibody/product/Goat-anti-Rabbit-IgG-H-L-Highly-Cross-Adsorbed-Secondary-Antibody-Polyclonal/A32732>

## Eukaryotic cell lines

Policy information about [cell lines and Sex and Gender in Research](#)

Cell line source(s)	Human primary stromal cells were extracted from the endometrium of both young and aging women using collagenase-I and DNase I treatment. Stromal cells were then cultured for one generation in preparation for artificial decidualization induction.
Authentication	Isolated stromal cells were identified by vimentin staining.
Mycoplasma contamination	Isolated stromal cells were not tested for mycoplasma contamination.
Commonly misidentified lines (See <a href="#">ICLAC</a> register)	No commonly misidentified lines exist.

## Palaeontology and Archaeology

Specimen provenance	n/a
Specimen deposition	n/a
Dating methods	n/a
<input type="checkbox"/> Tick this box to confirm that the raw and calibrated dates are available in the paper or in Supplementary Information.	
Ethics oversight	n/a

Note that full information on the approval of the study protocol must also be provided in the manuscript.

## Animals and other research organisms

Policy information about [studies involving animals](#); [ARRIVE guidelines](#) recommended for reporting animal research, and [Sex and Gender in Research](#)

Laboratory animals	8-week-old and 10-month-old C57BL/6J mice were acquired from Beijing Vital River Laboratory Animal Technology (Beijing, China). All mice were kept in a controlled environment with a 12-hour light/dark cycle, a room temperature of 20-25 °C, humidity of 55%±10%, and had access to food and water at all times.
Wild animals	No wild animals were used in this study.

Reporting on sex	All the mice were female.
Field-collected samples	No field-collected samples were used in this study.
Ethics oversight	All of the experimental procedures followed the guidelines of NIH for the Care and Use of Laboratory Animals. This study was approved by the Ethics Committee of Reproductive Medicine, Peking University Third Hospital.

Note that full information on the approval of the study protocol must also be provided in the manuscript.

## Clinical data

Policy information about [clinical studies](#)

All manuscripts should comply with the ICMJE [guidelines for publication of clinical research](#) and a completed [CONSORT checklist](#) must be included with all submissions.

Clinical trial registration	As a retrospective study, no clinical trial registration was performed.
Study protocol	The clinical data used in this study was from a retrospective observational study design. We collected the clinical information of 1,149 patients who had undergone preimplantation genetic testing for aneuploidy (PGT-A) screening at the Center for Reproductive Medicine of Peking University Third Hospital. After excluding possible impacts of abnormal embryos, the rates of biochemical pregnancy, clinical pregnancy, and live birth were significantly lower in women over 35 years old compared to those under 35.
Data collection	Baseline and pregnancy outcome data were collected from patients undergoing PGT-A screening at the Center for Reproductive Medicine, Peking University Third Hospital.
Outcomes	The primary outcome was full-term pregnancy. The secondary outcomes were biochemical pregnancy, clinical pregnancy, intrauterine pregnancy, pregnancy loss, and ongoing pregnancy.

## Dual use research of concern

Policy information about [dual use research of concern](#)

### Hazards

Could the accidental, deliberate or reckless misuse of agents or technologies generated in the work, or the application of information presented in the manuscript, pose a threat to:

- | No                                  | Yes                      |                            |
|-------------------------------------|--------------------------|----------------------------|
| <input checked="" type="checkbox"/> | <input type="checkbox"/> | Public health              |
| <input checked="" type="checkbox"/> | <input type="checkbox"/> | National security          |
| <input checked="" type="checkbox"/> | <input type="checkbox"/> | Crops and/or livestock     |
| <input checked="" type="checkbox"/> | <input type="checkbox"/> | Ecosystems                 |
| <input checked="" type="checkbox"/> | <input type="checkbox"/> | Any other significant area |

### Experiments of concern

Does the work involve any of these experiments of concern:

- | No                                  | Yes                      |   |
|-------------------------------------|--------------------------|---|
| <input checked="" type="checkbox"/> | <input type="checkbox"/> | Demonstrate how to render a vaccine ineffective                             |
| <input checked="" type="checkbox"/> | <input type="checkbox"/> | Confer resistance to therapeutically useful antibiotics or antiviral agents |
| <input checked="" type="checkbox"/> | <input type="checkbox"/> | Enhance the virulence of a pathogen or render a nonpathogen virulent        |
| <input checked="" type="checkbox"/> | <input type="checkbox"/> | Increase transmissibility of a pathogen                                     |
| <input checked="" type="checkbox"/> | <input type="checkbox"/> | Alter the host range of a pathogen  |
| <input checked="" type="checkbox"/> | <input type="checkbox"/> | Enable evasion of diagnostic/detection modalities                           |
| <input checked="" type="checkbox"/> | <input type="checkbox"/> | Enable the weaponization of a biological agent or toxin                     |
| <input checked="" type="checkbox"/> | <input type="checkbox"/> | Any other potentially harmful combination of experiments and agents         |

## Plants

Seed stocks

n/a

Novel plant genotypes

n/a

Authentication

n/a

## ChIP-seq

### Data deposition

- Confirm that both raw and final processed data have been deposited in a public database such as [GEO](#).
- Confirm that you have deposited or provided access to graph files (e.g. BED files) for the called peaks.

Data access links

*May remain private before publication.*

CUT&Tag data have been uploaded to the Genome Sequence Archive (accession number: HRA007501).  
 BED files of CUT&Tag data have been uploaded to the Open Archive for Miscellaneous Data (accession number: OMIX008964).

Files in database submission

Stromal-H3K27ac-aging-1.R1.fq.gz  
 Stromal-H3K27ac-aging-1.R2.fq.gz  
 Stromal-H3K27ac-aging-2.R1.fq.gz  
 Stromal-H3K27ac-aging-2.R2.fq.gz  
 Stromal-H3K27ac-aging-3.R1.fq.gz  
 Stromal-H3K27ac-aging-3.R2.fq.gz  
 Stromal-H3K27ac-young-1.R1.fq.gz  
 Stromal-H3K27ac-young-1.R2.fq.gz  
 Stromal-H3K27ac-young-2.R1.fq.gz  
 Stromal-H3K27ac-young-2.R2.fq.gz  
 Stromal-H3K27ac-young-3.R1.fq.gz  
 Stromal-H3K27ac-young-3.R2.fq.gz  
 Epithelial-H3K27ac-aging-1.R1.fq.gz  
 Epithelial-H3K27ac-aging-1.R2.fq.gz  
 Epithelial-H3K27ac-aging-2.R1.fq.gz  
 Epithelial-H3K27ac-aging-2.R2.fq.gz  
 Epithelial-H3K27ac-aging-3.R1.fq.gz  
 Epithelial-H3K27ac-aging-3.R2.fq.gz  
 Epithelial-H3K27ac-young-1.R1.fq.gz  
 Epithelial-H3K27ac-young-1.R2.fq.gz  
 Epithelial-H3K27ac-young-2.R1.fq.gz  
 Epithelial-H3K27ac-young-2.R2.fq.gz  
 Epithelial-H3K27ac-young-3.R1.fq.gz  
 Epithelial-H3K27ac-young-3.R2.fq.gz  
 Stromal-PR-aging-1.R1.fq.gz  
 Stromal-PR-aging-1.R2.fq.gz  
 Stromal-PR-aging-2.R1.fq.gz  
 Stromal-PR-aging-2.R2.fq.gz  
 Stromal-PR-aging-3.R1.fq.gz  
 Stromal-PR-aging-3.R2.fq.gz  
 Stromal-PR-young-1.R1.fq.gz  
 Stromal-PR-young-1.R2.fq.gz  
 Stromal-PR-young-2.R1.fq.gz  
 Stromal-PR-young-2.R2.fq.gz  
 Stromal-PR-young-3.R1.fq.gz  
 Stromal-PR-young-3.R2.fq.gz  
 H3K27ac-stromal-aging1.bed  
 H3K27ac-stromal-aging2.bed  
 H3K27ac-stromal-aging3.bed  
 H3K27ac-stromal-young1.bed  
 H3K27ac-stromal-young2.bed  
 H3K27ac-stromal-young3.bed  
 PGR-stromal-aging1.bed  
 PGR-stromal-aging2.bed  
 PGR-stromal-aging3.bed  
 PGR-stromal-young1.bed

PGR-stromal-young2.bed  
PGR-stromal-young3.bed

Genome browser session  
(e.g. [UCSC](#))

No genome browser session was available.

## Methodology

Replicates	Each experiment was repeated three times.
Sequencing depth	Purified PCR products were assessed using the Agilent 2100 Bioanalyzer. Libraries were sequenced on the Illumina NovaSeq 6000 platform, generating 150 bp paired-end reads. The total number of reads was from 37,949,441 to 47,994,878.
Antibodies	Acetyl-Histone H3 (Lys27) (D5E4) XP® Rabbit mAb, Cell signaling Technology, USA, Cat#8173S, 1:50 dilution. Progesterone Receptor A/B (D8Q2J) XP® Rabbit mAb, Cell signaling Technology, USA, Cat#8757T, 1:50 dilution.
Peak calling parameters	MACS2 was used to call the 'narrowPeak' using parameters -q 0.01 --nomodel --keep-dup auto. Sequences located within 400 bp of the peak summit were extracted, with any sequences containing significant repeat elements (as reported by RepeatMask) being excluded.
Data quality	The raw data was trimmed by fastp. Trimmed reads were aligned to the human reference genome hg38 using Bowtie2. After peak calling and merging, we obtained 30,420 H3K27ac peaks and 28,137 PGR peaks in young stromal cells, 14,256 H3K27ac peaks and 3,404 PGR peaks in aging stromal cells, 8,476 H3K27ac peaks in young epithelial cells, 2,152 H3K27ac peaks in aging epithelial cells.
Software	fastp (version 0.20.1), Bowtie2 (version 2.5.1), MACS2 (version 2.2.9.1), CHIPseeker (version 1.36.0), Homer (version 4.11), Diffbind (version 3.12.0).